Chapter 6

Rotating Cylinders, Annuli, and Spheres

Flow over rotating cylinders is important in a wide number of applications from shafts and axles to spinning projectiles. Also considered here is the flow in an annulus formed between two concentric cylinders where one or both of the cylindrical surfaces is or are rotating. As with the rotating flow associated with discs, the proximity of a surface can significantly alter the flow structure.

6.1. INTRODUCTION

An indication of the typical flow configurations associated with rotating cylinders and for an annulus with surface rotation is given in Figure 6.1. For the examples given in 6.1a, 6.1c, 6.1e, 6.1g, and 6.1i, a superposed axial flow is possible, resulting typically in a skewed, helical flow structure.

This chapter describes the principal flow phenomena, and develops and presents methods to determine parameters such as the drag associated with a rotating cylinder and local flow velocities. Flow for a rotating cylinder is considered in Section 6.2. Laminar flow between two rotating concentric cylinders, known as rotating Couette flow, is considered in Section 6.3. Rotation of annular surfaces can lead to instabilities in the flow and the formation of complex toroidal vortices, known, for certain flow conditions, as Taylor vortices. Taylor vortex flow represents a significant modeling challenge and has been subject to a vast number of scientific studies. The relevance of these to practical applications stems from the requirement to avoid Taylor vortex flow, the requirement to determine or alter fluid residence time in chemical processing applications, and the desire to understand fluid flow physics and develop and validate fluid flow models. Flow instabilities in an annulus with surface rotation and Taylor vortex flow are considered in Section 6.4. One of the most important practical applications of rotating flow is the journal bearing. Rotation can lead to the development of high pressures in a lubricant and the separation of shaft and bearing surfaces, thereby reducing wear. The governing fluid flow equation is called the Reynolds equation, and this equation, along with a

Rotating Flow, DOI: 10.1016/B978-0-12-382098-3.00006-8

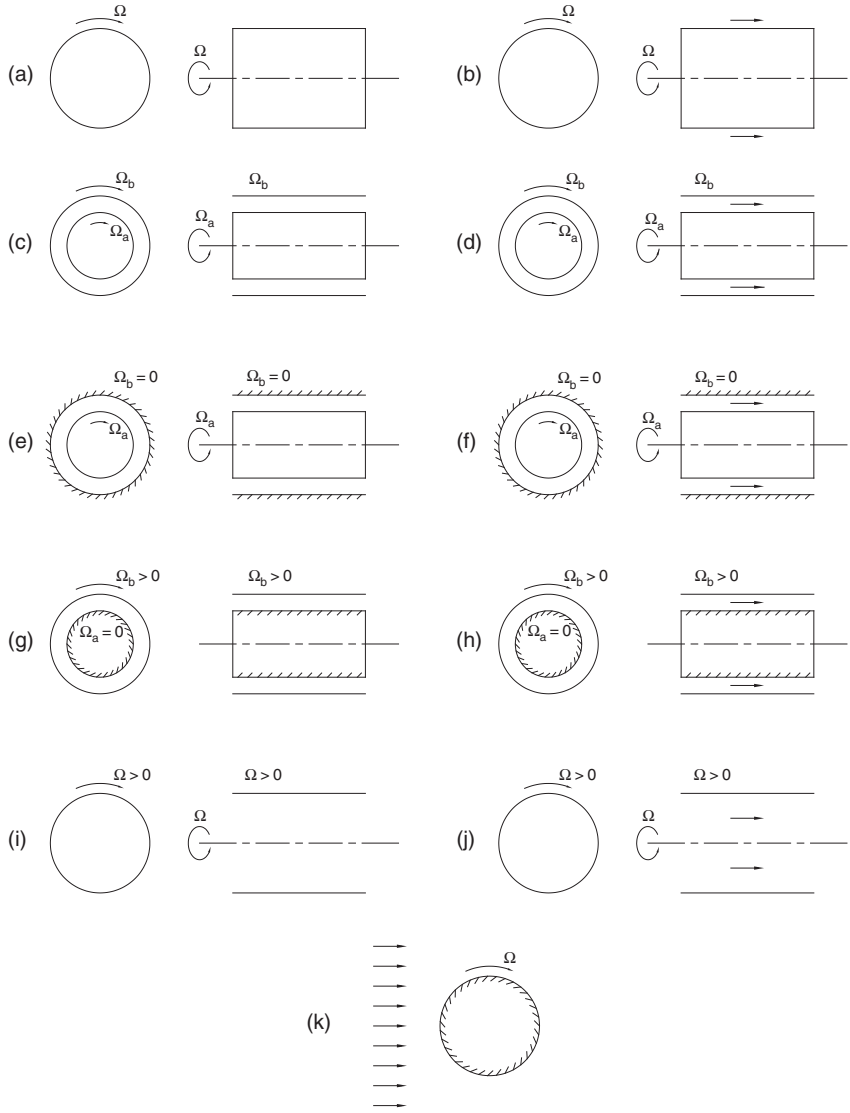

FIGURE 6.1 Selected cylinder and annulus flow configurations: (a) rotating cylinder, (b) rotating cylinder with superposed axial flow, (c) annulus with inner and outer cylinder rotation, (d) annulus with inner and outer cylinder rotation and throughflow, (e) annulus with inner cylinder rotation, (f) annulus with inner cylinder rotation and axial throughflow, (g) annulus with outer cylinder rotation, (h) annulus with outer cylinder rotation and axial throughflow, (i) internal flow within a rotating cylinder, (j) internal flow within a rotating cylinder with axial throughflow, (k) rotating cylinder with superposed cross-flow.

procedure for hydrodynamic bearing design, is developed in Section 6.5. A rotating cylinder with cross flow, along with the related case of a spinning sphere in a cross flow, is considered in Section 6.6.

6.2. ROTATING CYLINDER FLOW

A boundary layer will form on a rotating body of revolution due to the no-slip condition at the body surface as illustrated in Figure 6.2. At low values of the rotational Reynolds number, the flow will be laminar. As the rotational Reynolds number rises, the flow regime will become transitional and then turbulent. The approximate limit for laminar flow is for a rotational Reynolds number somewhere between 40 and 60.

The flow about a body of revolution rotating about its axis and simultaneously subjected to a flow in the direction of the axis of rotation is relevant to a number of applications, including certain rotating machinery and the ballistics of projectiles with spin. Various parameters such as the drag, moment coefficient, and the critical Reynolds number are dependent on the ratio of the circumferential to free-stream velocity. For example, the drag tends to increase with this ratio. The physical reason for this dependency is due to processes in the boundary layer where the fluid due to the no-slip condition co-rotates in the immediate vicinity of the wall and is therefore subject to the influence of strong "centrifugal forces." As a result, the processes of separation and transition from laminar to turbulent flow are affected by these forces and therefore drag too.

The boundary layer on a rotating body of revolution in an axial flow consists of the axial component of velocity and the circumferential component due to the

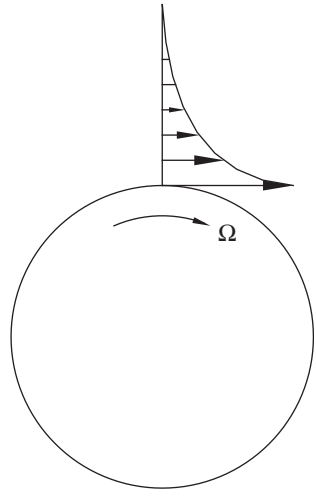

FIGURE 6.2 Boundary layer flow over a rotating cylinder.

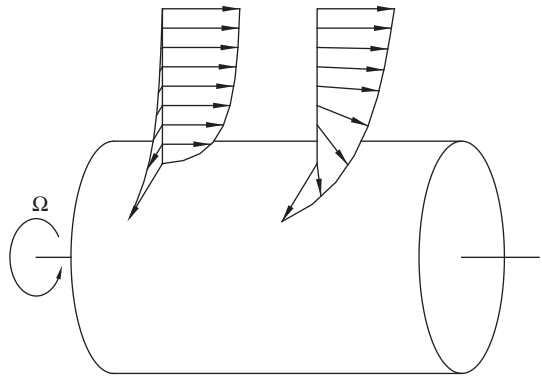

FIGURE 6.3 Boundary layer flow over a rotating cylinder with superposed axial flow.

no-slip condition at the body surface. The result is a skewed boundary layer as illustrated in Figure 6.3 for the case of a cylindrical body.

The thickness of the boundary layer increases as a function of the rotation parameter, λ_m, which is given by

$$\lambda_m = \frac{\Omega a}{u_{z,\infty}} \tag{6.1}$$

where Ω is the angular velocity of the cylinder, a is the radius of the cylinder, and $u_{z,\infty}$ is the free-stream axial velocity.

Steinheuer (1965) found the following relationship between the axial and rotational velocity for the boundary on a rotating cylinder with axial flow

$$\frac{u_\phi}{\Omega a} = 1 - \frac{u_z}{u_{z,\infty}} \tag{6.2}$$

A common requirement in practical applications is the need to quantify the power required to overcome the frictional drag of a rotating shaft. The moment coefficient for a rotating cylinder can be expressed by

$$C_{mc} = \frac{T_q}{0.5\pi\rho\Omega^2 a^4 L} \tag{6.3}$$

where a, L, and Ω are the radius, length, and angular velocity of the cylinder, respectively, as illustrated in Figure 6.4.

For laminar flow, Lamb (1932) gives the moment coefficient for a rotating cylinder, based on the definition given in Equation 6.3, as

$$C_{mc} = \frac{8}{\mathrm{Re}_\phi} \tag{6.4}$$

Extensive experiments on rotating cylinders for the case of both laminar and turbulent flow were undertaken by Theodorsen and Regier (1944) for a range of

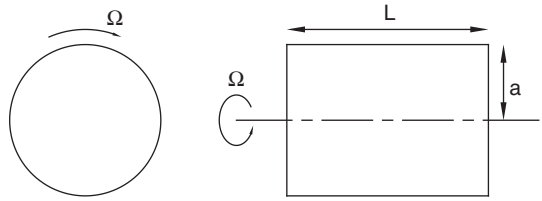

FIGURE 6.4 Rotating cylinder principal dimensions.

cylinders with diameters ranging from 12.7 mm to 150 mm and lengths between 150 mm and 1.2 m in oil, kerosene, water and air at rotational Reynolds numbers up to approximately 5.6×10^6. The data follow the laminar trend within approximately 15% up to a rotational Reynolds number of approximately 60. An empirical correlation was produced for turbulent flow for smooth cylinders, with the contribution due to the end discs removed, given in Equation 6.5.

$$\frac{1}{\sqrt{C_{mc}}} = -0.8572 + 1.250\ln(\mathrm{Re}_\phi \sqrt{C_{mc}}) \tag{6.5}$$

It is not possible to separate out the moment coefficient algebraically; this equation must be solved using an iterative technique for a given rotational Reynolds number. Equation 6.5 is restated in Equation 6.6, and a starting value of, say, $C_{mc} = 0.02$ generally results in a converged solution to within three significant figures within about four or five iterations.

$$C_{mc} = \left(\frac{1}{-0.8572 + 1.25\ln(\mathrm{Re}_\phi \sqrt{C_{mc}})}\right)^2 \tag{6.6}$$

Values for the drag coefficient as a function of the rotational Reynolds number for both Equations 6.4 and 6.6 are presented in Figure 6.5.

The power required to overcome frictional drag can be determined by

$$Power = T_q \times \Omega \tag{6.7}$$

Substituting for the torque in Equations 6.7 using Equation 6.3 gives

$$Power = 0.5\pi\rho\Omega^3 a^4 L C_{mc} \tag{6.8}$$

The power required to overcome frictional drag for a rotating cylinder as a function of a rotational Reynolds number for a range of radii between 40 mm and 400 mm, assuming a cylinder length of 0.4 m and a density of 1.2047 kg/m^3, are presented in Figure 6.6. For the case of a rotating drum with end discs, the contribution to the overall power requirement to overcome frictional drag due to the rotating discs would also need to be accounted for, and the techniques presented in Chapters 4 and 5 can be adopted as appropriate.

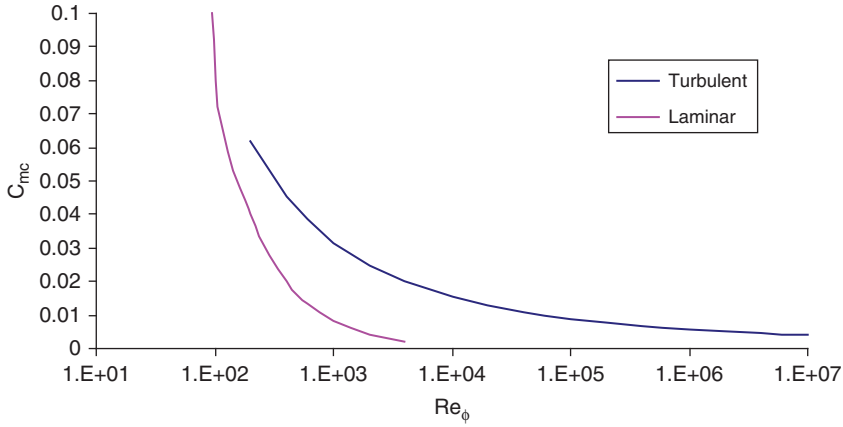

FIGURE 6.5 Moment coefficients for a rotating cylinder as a function of the rotational Reynolds number.

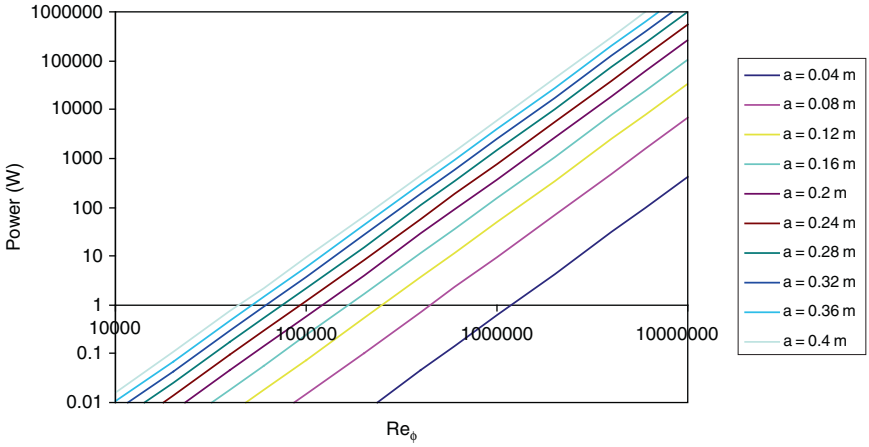

FIGURE 6.6 Power requirement for a smooth rotating cylinder, of length 400 mm in air with density 1.2047 kg/m^3.

Example 6.1.

Determine the power required to overcome frictional drag for a 250-mm-long shaft with a diameter of 100 mm rotating at 10,500 rpm in air with a density and viscosity of 4 kg/m^3 and 3 $\times$ 10^{-5} Pa s, respectively. Compare the figure for the frictional drag to that of the power required to overcome frictional drag for both the discs and the bolts for the disc also spinning at 10,500 rpm in Example 5.4, Chapter 5.

Solution

The rotational Reynolds number for the shaft, from Equation (4.1), is

$$\mathrm{Re}_{\phi} = \frac{\rho \Omega b^2}{\mu} = \frac{4 \times 1100 \times 0.05^2}{3 \times 10^{-5}} = 3.667 \times 10^5$$

This value is significantly higher than 60, so the flow can be taken to be turbulent.

Assuming an initial guess for the moment coefficient in Equation 6.6 of $C_{mc} = 0.02$,

$$C_{mc} = \left(\frac{1}{-0.8572 + 1.25 \ln(3.667 \times 10^5 \sqrt{0.02})} \right)^2 = 0.006187$$

Using the updated value for the moment coefficient in Equation 6.6

$$C_{mc} = \left(\frac{1}{-0.8572 + 1.25 \ln(3.667 \times 10^5 \sqrt{0.006187})} \right)^2 = 0.006968$$

Using the updated value for the moment coefficient in Equation 6.6

$$C_{mc} = \left(\frac{1}{-0.8572 + 1.25 \ln(3.667 \times 10^5 \sqrt{0.006968})} \right)^2 = 0.006882$$

Using the updated value for the moment coefficient in Equation 6.6

$$C_{mc} = \left(\frac{1}{-0.8572 + 1.25 \ln(3.667 \times 10^5 \sqrt{0.006882})} \right)^2 = 0.006891$$

Using the updated value for the moment coefficient in Equation 6.6

$$C_{mc} = \left(\frac{1}{-0.8572 + 1.25 \ln(3.667 \times 10^5 \sqrt{0.006891})} \right)^2 = 0.006890$$

This value is within one significant figure of the previous value and can be assumed to be converged.

The power required to overcome frictional drag, using Equation 6.8 is given by

$$\text{Power} = 0.5 \times \pi \times 4 \times 1100^3 \times 0.05^4 \times 0.25 \times 0.006890 \approx 90 \text{ W}$$

The power required to over frictional drag for the rotating shaft is comparatively small, less than 1% of that required to overcome the frictional drag for both the disc face and the bolts for the disc configuration of Example 5.4.

Example 6.2.

Determine the power required to overcome frictional drag for a 300-mm-long shaft with a diameter of 120 mm rotating at 15,000 rpm in air with a density and viscosity of 5.2 kg/m^3 and 3×10^{-5} Pa s, respectively.

Solution

The rotational Reynolds number for the shaft, from Equation 4.1, is

$$\mathrm{Re}_\phi = \frac{\rho \Omega b^2}{\mu} = \frac{5.2 \times 1571 \times 0.06^2}{3 \times 10^{-5}} = 9.80 \times 10^5$$

This value is significantly higher than 60, so the flow can be taken to be turbulent.

Assuming an initial guess for the moment coefficient in Equation 6.6 of $C_{mc} = 0.02$,

$$C_{mc} = \left(\frac{1}{-0.8572 + 1.25 \ln(9.80 \times 10^5 \sqrt{0.02})} \right)^2 = 0.005144$$

Using the updated value for the moment coefficient in Equation 6.6

$$C_{mc} = \left(\frac{1}{-0.8572 + 1.25 \ln(9.80 \times 10^5 \sqrt{0.005144})} \right)^2 = 0.005833$$

Using the updated value for the moment coefficient in Equation 6.6

$$C_{mc} = \left(\frac{1}{-0.8572 + 1.25 \ln(9.80 \times 10^5 \sqrt{0.005833})} \right)^2 = 0.005764$$

Using the updated value for the moment coefficient in Equation 6.6

$$C_{mc} = \left(\frac{1}{-0.8572 + 1.25 \ln(9.80 \times 10^5 \sqrt{0.005764})} \right)^2 = 0.005770$$

Using the updated value for the moment coefficient in Equation 6.6

$$C_{mc} = \left(\frac{1}{-0.8572 + 1.25 \ln(9.80 \times 10^5 \sqrt{0.005770})} \right)^2 = 0.005769$$

This value is within one significant figure of the previous value and can be assumed to be converged.

The power required to overcome frictional drag, using Equation 6.8, is given by

$$\text{Power} = 0.5 \times \pi \times 5.2 \times 1571^3 \times 0.06^4 \times 0.3 \times 0.005769 = 710.4 \text{ W}$$

In this case, the power required to overcome frictional drag for the rotating shaft is quite significant, and as in most rotating machines, putting heat into the fluid surrounding a shaft is an unwanted side effect that generally needs to be minimized by minimizing the radius of the shaft and its length.

For rough cylinders, Theodorsen and Regier (1944) found that the moment coefficient was dependent on the relative grain size and grain spacing applied to the cylinder surface, and that beyond a critical Reynolds number the drag coefficient remains constant and independent of the rotational Reynolds number. For

$$e > 3.3\frac{\nu}{\sqrt{\tau_o/\rho}} \tag{6.9}$$

where e is the roughness grain size and τ_o is the shear stress at the surface, the moment coefficient is given by

$$\frac{1}{\sqrt{C_{mc}}} = 1.501 + 1.250\ln\frac{a}{e} \tag{6.10}$$

The center line average roughness, R_a, is related to the sand-grain roughness by $R_a \approx k_s/2$ (see Childs and Noronha, 1997), allowing the following substitution.

$$\frac{1}{\sqrt{C_{mc}}} = 0.8079 + 1.250\ln\frac{a}{R_a} \tag{6.11}$$

6.3. ROTATING COUETTE FLOW

The term *Couette flow* describes flow between two surfaces that are in close proximity, such that flow is dominated by viscous effects and inertial effects are negligible. In cylindrical coordinates this involves flow in an annulus, as illustrated in Figure 6.7, and the Navier-Stokes equations can be solved exactly by analytical techniques, subject to a number of significant assumptions, which severely limit the application of the resulting solution. Nevertheless, the approach is instructive and also forms the basis for a technique to determine the viscosity of fluid.

The analysis presented here for rotating Couette flow assumes laminar flow and is valid provided the Taylor number given in a form based on the mean annulus radius in Equation 6.12, is less than the critical Taylor number, Ta_{cr}. If the critical Taylor number is exceeded, toroidal vortices can be formed in the annulus. The formation of such vortices is considered in Section 6.4. The critical Taylor number is dependent on a number of factors, including the rotation ratio and annulus dimensions. For the case of a narrow gap annulus, with a stationary outer cylinder the critical Taylor number is 41.19.

$$Ta_m = \frac{\Omega r_m^{0.5}(b-a)^{1.5}}{\nu} \tag{6.12}$$

where $r_m = (a + b)/2$.

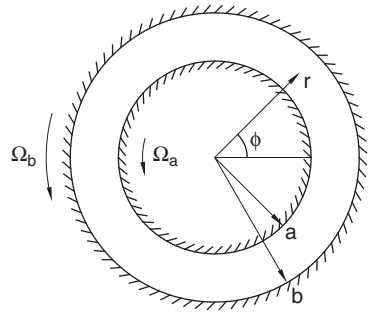

FIGURE 6.7 Rotating Couette flow.

If the flow is assumed to be contained between two infinite concentric cylinders, as illustrated in Figure 6.7, with either cylinder rotating at speed Ω_a and $\Omega_{b,}$ respectively, with no axial or radial flow under steady conditions, the continuity equation reduces to Equation 6.13 and the radial and tangential and components of the Navier-Stokes equations reduce to Equations 6.14 and 6.15.

$$\frac{\partial u_\phi}{\partial \phi} = 0 \tag{6.13}$$

$$-\frac{\rho u_\phi^2}{r} = -\frac{dp}{dr} \tag{6.14}$$

$$0 = \mu\left(\frac{d^2u_\phi}{dr^2} + \frac{1}{r}\frac{du_\phi}{dr} - \frac{u_\phi}{r^2}\right) \tag{6.15}$$

or

$$\frac{d^2u_\phi}{dr^2} + \frac{d}{dr}\left(\frac{u_\phi}{r}\right) = 0 \tag{6.16}$$

These equations can be solved with appropriate boundary conditions to give the velocity distribution as a function of radius and the torque on the inner and outer cylinders:

The boundary conditions are as follows:

at $r = a$, $u_\phi = \Omega a$

at $r = b$, $u_\phi = \Omega b$, and $p = p_b$

Equation 6.16 is in the familiar form of an ordinary differential equation, which has a standard solution of the form

$$u_\phi = C_1 r + \frac{C_2}{r} \tag{6.17}$$

The constants C_1 and C_2 are given by

$$C_1 = \frac{\Omega_b b^2 - \Omega_a a^2}{b^2 - a^2} \tag{6.18}$$

$$C_2 = \frac{(\Omega_a - \Omega_b)a^2 b^2}{b^2 - a^2} \tag{6.19}$$

The velocity given in Equation 6.17 can be substituted in Equation 6.14 to give the pressure distribution

$$\frac{dp}{dr} = \rho\left(C_1^2 r + \frac{2C_1C_2}{r} + \frac{C_2^2}{r^3}\right) \tag{6.20}$$

This equation can be integrated giving

$$p = \rho\left(C_1^2\frac{r^2}{2} + 2C_1C_2\ln r - \frac{C_2^2}{2r^2}\right) + C \tag{6.21}$$

where the constant of integration C can be evaluated by specifying the value of pressure $p = p_a$ at $r = a$ or $p = p_b$ at $r = b$ for any particular problem.

The viscous shear stress at $r = a$ is given by

$$\tau = \mu\frac{r\partial(u_\phi/r)}{\partial r} \tag{6.22}$$

Hence for $r = a$, from Equations 6.17 and 6.19

$$\tau = -2\mu\frac{C_2}{r^2} = -2\mu\frac{C_2}{a^2} = -2\mu\frac{(\Omega_a - \Omega_b)b^2}{b^2 - a^2} \tag{6.23}$$

The torque per unit length L is equal to $\tau Aa/L$. The surface area of the cylinder is $2\pi aL$, so the torque per unit length is

$$T_q = \frac{\tau(2\pi aL)a}{L} = 2\pi a^2\tau \tag{6.24}$$

Substituting for the shear stress from Equation 6.23 gives the torque per unit length as

$$T_q = 4\pi\mu\frac{a^2b^2}{b^2 - a^2}(\Omega_b - \Omega_a) \tag{6.25}$$

Similarly, the torque per unit length for the outer cylinder is given by

$$T_q = -4\pi\mu\frac{a^2b^2}{b^2 - a^2}(\Omega_b - \Omega_a) \tag{6.26}$$

It should be noted that these equations for the torque per unit length are valid only if the flow remains entirely circumferential.

It is possible to make use of Equation 6.26 in the measurement of viscosity, known as viscometry, using a device made up of two concentric cylinders, arranged vertically with height L, with the test substance held between the cylinders (Mallock, 1888, 1896; Couette, 1890). The inner cylinder is locked in a stationary position and the outer cylinder is rotated as indicated in Figure 6.8.

From measurements of the angular velocity of the outer cylinder and the torque on the inner cylinder, the viscosity can be determined, as in Equation 6.27.

$$\mu = \left|T_q\frac{b^2 - a^2}{4\pi\Omega_b a^2 b^2 L}\right| \tag{6.27}$$

Bilgen and Boulos (1973) give the following equation for the moment coefficient for an annulus with inner cylinder rotation with no axial pressure gradient for laminar flow.

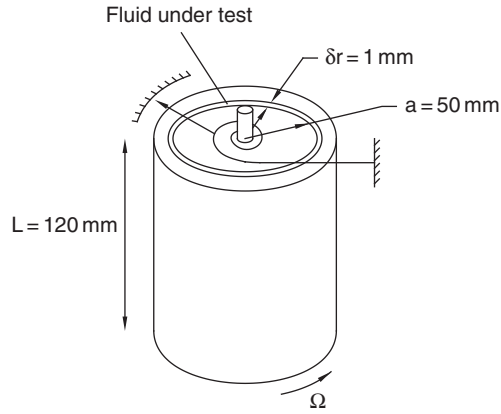

FIGURE 6.8 Typical viscometer.

$$C_{mc} = 10\left(\frac{b-a}{a}\right)^{0.3} \mathrm{Re}_{\phi m}^{-1} \tag{6.28}$$

where the rotational Reynolds number, $Re_{\phi m}$, is based on the annulus gap,

$$\mathrm{Re}_{\phi m} = \frac{\rho \Omega a(b-a)}{\mu} \tag{6.29}$$

for

$$\mathrm{Re}_{\phi m} < 64 \tag{6.30}$$

The equivalent relationship for the moment coefficient from the linear theory, Equations 6.3 and 6.25, is

$$C_{mc} = \frac{8b^2}{b^2-a^2}\mathrm{Re}_{\phi}^{-1} = \frac{8b^2}{a(b+a)}\mathrm{Re}_{\phi m}^{-1} \tag{6.31}$$

Equation 6.28 compares favorably with Equation 6.31. Bilgen and Boulos (1973) report that the maximum mean deviation of Equation 6.28 from their experimental data was $\pm 5.8\%$.

Example 6.3.

Determine the power required to overcome frictional drag for a cylinder with a radius of 0.25 m rotating at 10 revolutions per minute within an annulus, with the outer cylinder rotating if the length of the annulus is 0.4 m and the gap between the inner and outer cylinder is 5 mm. The annulus is filled with oil of viscosity 0.02 Pa s and density 900 kg/m^3.

Solution

The rotational Reynolds number from Equation 6.29 is

$$\mathrm{Re}_{\phi m} = \frac{\rho \Omega a(b-a)}{\mu} = \frac{900 \times 10 \times (2\pi/60) \times 0.25 \times 0.005}{0.02} = 58.9$$

As this is less than 64, the empirical correlation given in Equation 6.28 can be used.

$$C_{mc} = 10\left(\frac{b-a}{a}\right)^{0.3} \mathrm{Re}_{\phi m}^{-1} = 10\left(\frac{0.005}{0.25}\right)^{0.3} (58.9)^{-1} = 0.0525$$

The power required to overcome frictional drag, from Equation 6.8 is

$$Power = 0.5\pi\rho\Omega^3 a^4 L C_{mc} = 0.5\pi \times 900 \times 1.047^3 \times 0.25^4 \times 0.4 \times 0.0525 = 0.1331\ \mathrm{W}$$

Example 6.4.

The torque indicated by a viscometer is 0.01 N m. If the diameter of the inner cylinder is 100 mm, the annular gap is 1 mm, the length is 120 mm, and the outer cylinder rotates at 40 rpm, determine the viscosity of the fluid contained in the viscometer.

Solution

The angular velocity of the outer cylinder is

$$\Omega_b = 40 \times \frac{2\pi}{60} = 4.188\ \mathrm{rad/s}$$

From Equation 6.27,

$$\mu = T_q \frac{b^2 - a^2}{4\pi\Omega_b a^2 b^2 L} = 0.01 \frac{0.051^2 - 0.05^2}{4\pi \times 4.188 \times 0.05^2 \times 0.051^2 \times 0.12} = 0.02459\ \mathrm{Pa\ s}$$

Examination of the tangential velocity in rotating Couette flow, Equation 6.17, yields a number of cases of special interest. For the case where the inner radius a and the angular velocity of the inner cylinder tend to zero, Equation 6.17 gives

$$u_\phi = \Omega_a r = \text{constant} \tag{6.32}$$

Equation 6.32 implies that rotation of a circular pipe filled with fluid will induce solid body motion of the fluid within it. If the outer cylinder becomes very large and does not rotate, then in the limit as $r \to \infty$ with $\Omega_b = 0$

$$u_\phi = \frac{a^2 \Omega_a}{r} \tag{6.33}$$

Equation 6.33 represents a potential or free vortex, driven in a viscous fluid by the no-slip condition. Equation 6.17, and hence Equation 6.33, were derived assuming an infinite annulus length. The fluid contained within an infinite annulus will therefore have infinite momentum. It therefore takes, in theory, an infinite length of time for potential vortex flow to be generated by rotation of the inner cylinder alone. Velocity distributions for the case of inner cylinder only rotation and outer cylinder only rotation are given in Figures 6.9 and 6.10 for a range of radius ratios *a/b*.

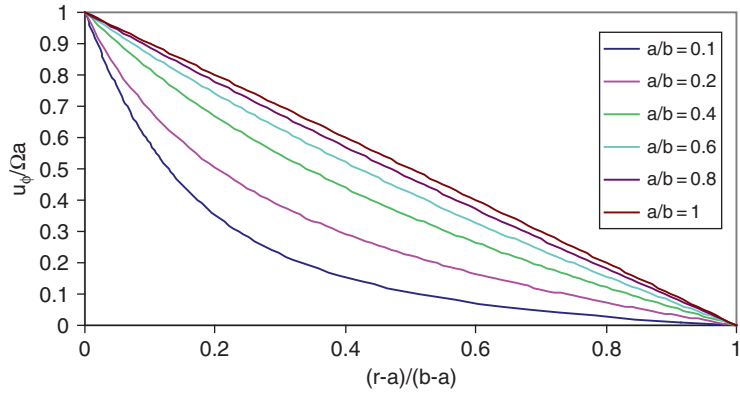

FIGURE 6.9 Velocity distribution for rotating Couette flow in a concentric annulus with inner cylinder only rotation for various values of radius ratio.

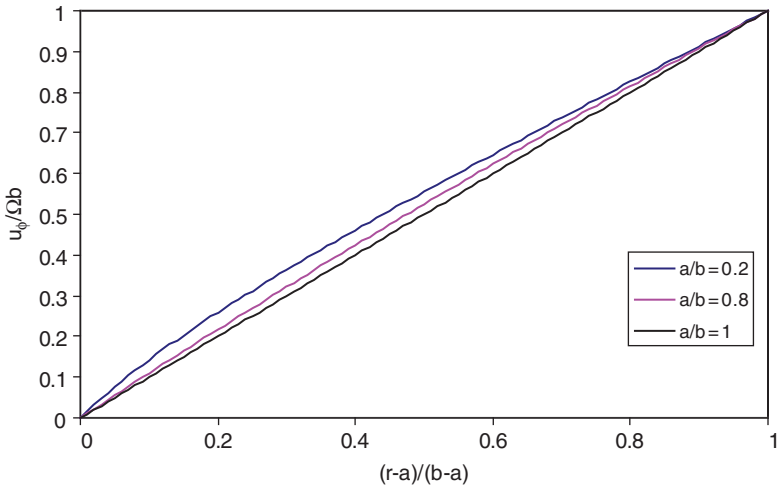

FIGURE 6.10 Velocity distribution for rotating Couette flow in a concentric annulus with outer cylinder only rotation.

Example 6.5.

Calculate the tangential velocity at a radius of 0.045 m for an annulus with an inner cylinder radius of 0.04 m and an annular gap of 0.01 m filled with oil with a density of 900 kg/m^3 and a viscosity of 0.022 Pa s for the following conditions.

i. The inner cylinder only is rotating with an angular velocity of 3 rad/s
ii. The outer cylinder only is rotating with an angular velocity of 3 rad/s
iii. If the inner and outer cylinders are rotating with angular velocities of 3 rad/s and 6 rad/s respectively

Solution

The rotational Reynolds number from Equation 6.29 is

$$\mathrm{Re}_{\phi m} = \frac{\rho \Omega a(b-a)}{\mu} = \frac{900 \times 3 \times 0.04 \times 0.01}{0.022} = 49.09$$

As this value is less than 64, the flow is likely to be laminar, and Equation 6.16 can be used to model the tangential velocity in the annulus.

(i) From Equation 6.18,

$$C_1 = \frac{\Omega_b b^2 - \Omega_a a^2}{b^2 - a^2} = \frac{\Omega_a a^2}{b^2 - a^2} = -\frac{3 \times 0.04^2}{0.05^2 - 0.04^2} = -5.333$$

From Equation 6.19,

$$C_2 = \frac{(\Omega_a - \Omega_b) a^2 b^2}{b^2 - a^2} = \frac{\Omega_a a^2 b^2}{b^2 - a^2} = \frac{3 \times 0.04^2 \times 0.05^2}{0.05^2 - 0.04^2} = 0.01333$$

Hence from Equation 6.17,

$$u_\phi = -5.333r + \frac{0.01333}{r}$$

So at $r = 0.045$ m,

$$u_\phi = -5.333 \times 0.045 + \frac{0.01333}{0.045} = 0.05624 \text{ m/s}$$

(ii) From Equation 6.18,

$$C_1 = \frac{\Omega_b b^2 - \Omega_a a^2}{b^2 - a^2} = \frac{\Omega_b a^2}{b^2 - a^2} = \frac{3 \times 0.05^2}{0.05^2 - 0.04^2} = 8.333$$

From Equation 6.19,

$$C_2 = \frac{(\Omega_a - \Omega_b) a^2 b^2}{b^2 - a^2} = -\frac{\Omega_b a^2 b^2}{b^2 - a^2} = -\frac{3 \times 0.04^2 \times 0.05^2}{0.05^2 - 0.04^2} = -0.01333$$

Hence from Equation 6.17,

$$u_\phi = 8.333r - \frac{0.01333}{r}$$

So at $r = 0.045$ m,

$$u_\phi = 8.333 \times 0.045 - \frac{0.01333}{0.045} = 0.0787 \text{ m/s}$$

(iii) From Equation 6.18,

$$C_1 = \frac{\Omega_b b^2 - \Omega_a a^2}{b^2 - a^2} = \frac{6 \times 0.05^2 - 3 \times 0.04^2}{0.05^2 - 0.04^2} = 11.33$$

From Equation 6.19,

$$C_2 = \frac{(\Omega_a - \Omega_b) a^2 b^2}{b^2 - a^2} = \frac{(3-6) \times 0.04^2 \times 0.05^2}{0.05^2 - 0.04^2} = -0.01333$$

Hence from Equation 6.17,

$$u_\phi = 11.33r - \frac{0.01333}{r}$$

So at $r = 0.045$ m,

$$u_\phi = 11.33 \times 0.045 - \frac{0.01333}{0.045} = 0.2137 \text{ m/s}$$

Example 6.6.

Determine the pressure at a radius of 0.045 m and at a radius of 0.041 m for the conditions of part (i) identified in the previous example if the pressure at the outer radius of the annulus is 1.12 bar absolute.

Solution

From Equation 6.21,

$$C = p_b - \rho \left(C_1^2 \frac{b^2}{2} + 2C_1 C_2 \ln b - \frac{C_2^2}{2b^2} \right)$$

$$= 1.12 \times 10^5 - 900 \left((-5.333)^2 \frac{0.05^2}{2} + 2 \times -5.333 \times 0.01333 \ln 0.05 - \frac{0.01333^2}{2 \times 0.05^2} \right)$$

$$= 111616.546 \text{ Pa}$$

(The result to three decimal places has been deliberately stated here for the constant of integration, C, in order to enable the variation of pressure with radius to be distinguished.)

From Equation 6.21 at a radius of $r = 0.045$ m,

$$p = 111999.9 \text{ Pa}$$

From Equation 6.21 at a radius of $r = 0.041$ m,

$$p = 111999.328 \text{ Pa}$$

(The result is stated to three decimal places in order to illustrate the subtle variation of static pressure with radius.)

6.4. FLOW INSTABILITIES AND TAYLOR VORTEX FLOW

The equations presented for Couette flow in an annulus with rotation characterize a system in which dynamic equilibrium exists between the radial forces and the radial pressure gradient. However, when it is not possible for the radial pressure gradient and the viscous forces to dampen out and restore changes in centrifugal forces caused by small disturbances in the flow, the fluid motion is unstable and results in a secondary flow. A simple criterion for determining the onset of inertial instability was developed by Rayleigh (1916).

The Rayleigh instability criterion examines the balance between radial forces and the radial pressure gradient in a circular pathline flow field in order to identify whether a displaced fluid has a tendency to return to its original location. In essence the criterion determines whether the force due to inward radial pressure is adequate to maintain inward centripetal acceleration for an arbitrary element of fluid.

In this analysis, an element of fluid is assumed to have been perturbed, or moved, to a new radius, quickly enough so that its original fluid properties, density, temperature, and so on, are maintained. In a Rayleigh stability analysis for a rotating flow, the property that is conserved is momentum.

Consider a toroidal element of rotating fluid contained initially between $r + dr$ and $z + dz$ which is displaced from an initial radius r_1 to a final radius r_2 such that $r_2 > r_1$. Local disturbances in a fluid can occur for many reasons from, for example, small-scale fluctuations in fluid properties and conditions, dirt in the flow, and vibration. At its new radial position, it will now be rotating faster than the new environment, and the radial pressure gradient associated with the flow will be insufficient to balance the radial acceleration associated with the displaced fluid element. As a result, the fluid will tend to move further outward, providing the mechanism for the unstable flow. In a similar manner, a fluid element at a smaller radius will tend to move radially inward.

This qualitative argument is repeated here in a quantitative form for an elemental toroid of fluid initially at radius r_1 with angular velocity Ω_1, which is displaced to a radius r_2 without interacting with the remainder of the fluid and ignoring the stabilizing tendency of viscosity.

Angular momentum is the product of linear moment and the perpendicular distance of the particle from the axis. Angular momentum must be conserved for an axisymmetric disturbance, so the velocities are related by

$$mu_{\phi 1} r_1 = mu_{\phi f} r_2 \tag{6.34}$$

or

$$m\Omega_1 r_1^2 = m\Omega_2 r_2^2 \tag{6.35}$$

The element's tangential velocity component after displacement will be

$$u_{\phi f} = \frac{u_{\phi 1} r_1}{r_2} \tag{6.36}$$

The centripetal acceleration of the displaced element of fluid is

$$-\frac{u_{\phi f}^2}{r_2} = -\left(\frac{u_{\phi 1} r_1}{r_2}\right)^2 \frac{1}{r_2} = -\frac{(u_{\phi 1} r_1)^2}{r_2^3} \tag{6.37}$$

The radial acceleration of the fluid element will be countered by the pressure gradient

$$\frac{\partial p}{\partial r} = -\rho \frac{u_{\phi 2}^2}{r_2} \tag{6.38}$$

So if the radial force of the fluid ring exceeds the pressure gradient, then the ring will have a tendency to continue moving outward and the associated motion will be unstable.
That is, if

$$\rho \frac{u_{\phi 1}^2 r_1^2}{r_2^3} > \rho \frac{u_{\phi 2}^2}{r_2} \tag{6.39}$$

or if

$$u_{\phi 1}^2 r_1^2 > u_{\phi 2}^2 r_2^2 \tag{6.40}$$

the flow will have a tendency to be unstable.

Conversely, the conditions for stability are if

$$\frac{u_{\phi 2}^2}{r_2} > \frac{(r_1 u_{\phi 1})^2}{r_2^3} \tag{6.41}$$

or

$$(r_2 u_{\phi 2})^2 > (r_1 u_{\phi 1})^2 \tag{6.42}$$

then the flow field is stable to the perturbation and a displaced element of fluid will return to its initial radius.

The condition for stability, that is,

$$\frac{d}{dr}(r u_\phi)^2 > 0 \tag{6.43}$$

or

$$\frac{d}{dr}|\Omega r^2| > 0 \tag{6.44}$$

is usually referred to as the Rayleigh criterion.

According to the Rayleigh criterion, an inviscid flow is thus unstable if the mean velocity distribution is such that the product $u_\phi r$ decreases radially outward with conservation of angular momentum about the axis of rotation.

Applying this to Couette flow, then for stability $\Omega_a > 0$. For two cylinders rotating in the same direction, the flow is either stable everywhere or unstable

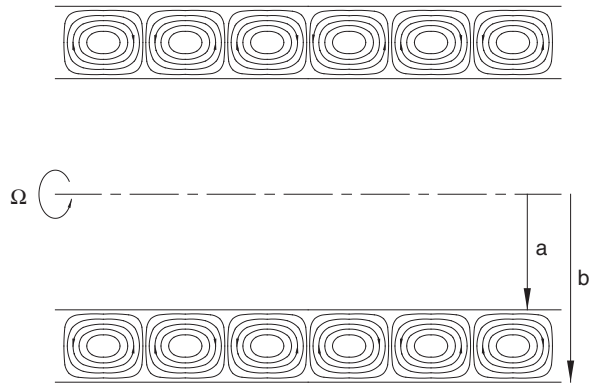

FIGURE 6.11 Taylor vortices.

everywhere. From the solution for the velocity distribution for Couette flow, $u_\phi = Ar + B/r$, then from Equation 6.44, gives

$$\frac{\Omega_b}{\Omega_a} > \left(\frac{a}{b}\right)^2 \tag{6.45}$$

or

$$\Omega_b b^2 > \Omega_a a^2 \tag{6.46}$$

For two cylinders rotating in opposite directions, the region close to the inner cylinder is unstable and the region close to the outer cylinder is stable.

The Rayleigh criterion based on the simple displaced particle concept provides an indication of the onset of instabilities. In real flows, the onset of instability is modified by the action of viscosity.

Experiments, for example, Taylor (1923), revealed that the simple axisymmetric laminar flow in an annulus with a combination of inner and outer cylinder rotation was replaced by a more complicated eddying flow structure. If the angular velocity exceeded a critical value, a steady axisymmetric secondary flow in the form of regularly spaced vortices in the axial direction, as illustrated in Figures 6.11 and 6.12, was generated. Alternate vortices rotate in opposite directions. The physical mechanism driving the vortices can be determined using insight from the Rayleigh stability criterion.

Considering the case of an annulus with the inner cylinder rotating at a higher speed than the outer cylinder, a fluid element at a low radius, if disturbed and forced radially outward, will have a radial outward force at its new radial location that will exceed the local radial pressure gradient. Thus the fluid element will have a tendency to continue to move with a net radial outward motion. Once it reaches the outer radius, it must go somewhere and will therefore flow along the outer cylinder. Continuity will cause particles to fill the space vacated the fluid element. The net result is the formation of a

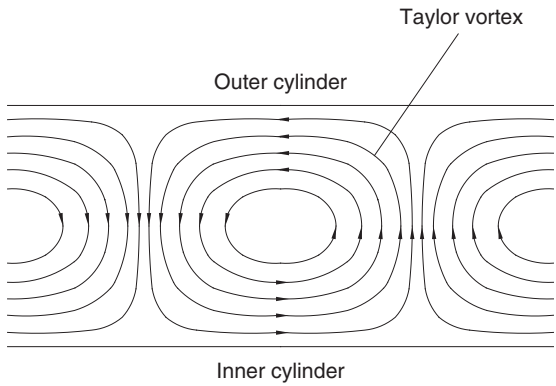

FIGURE 6.12 Taylor vortices cells.

circulating motion as indicated in Figure 6.12. The reasoning behind the multiple vortex cells is that if two fluid elements are both moving radially outward, then when they reach the outer radius, they cannot both go in the same direction along the outer cylinder; therefore the flow divides in opposite directions, causing two contra-rotating vortex cells to be formed.

Taylor (1923) formulated the stability problem taking into account the effects of viscosity by assuming an axisymmetric infinitesimal disturbance and solving the dynamic conditions under which instability occurs. Whereas the Rayleigh criterion, for the case where the outer cylinder is stationary, predicts that the flow for an inviscid fluid is unstable at infinitesimally small angular velocities of the inner cylinder, Taylor's linear stability analysis showed that viscosity delayed the onset of secondary flow.

Assuming the annular gap, $b - a$, is small compared to the mean radius, $r_m = (a + b)/2$, known as the small gap approximation, Taylor's solution for the angular velocity at which laminar flow breaks down and the flow instabilities grow leading to the formation of secondary flow vortices, called the critical speed, is given by

$$\Omega_{cr} = \pi^2 \nu \sqrt{\frac{(a+b)}{2S(b-a)^3 a^2 [1-(\Omega_b/\Omega_a) b^2/a^2](1-\Omega_b/\Omega_a)}} \tag{6.47}$$

where

$$S = 0.0571\left[\frac{1+\Omega_b/\Omega_a}{1-\Omega_b/\Omega_a} + 0.652\left(1-\frac{1}{x}\right)\right] + 0.00056\left[\frac{1+\Omega_b/\Omega_a}{1-\Omega_b/\Omega_a} + 0.652\left(1-\frac{1}{x}\right)\right]^{-1} \tag{6.48}$$

where $x = a/b$.

For the case of a stationary outer cylinder, $\Omega_b/\Omega_a = 0$, Equations 6.47 and 6.48 reduce to

$$\Omega_{cr} = \pi^2 \nu \sqrt{\frac{a+b}{2S(b-a)^3 a^2}} \tag{6.49}$$

$$S = 0.0571[1-0.652(b-a)/a] + 0.00056[1-0.652(b-a)/a]^{-1} \tag{6.50}$$

For the case of a narrow gap and stationary outer cylinder, $x \to 1$, $\Omega_b/\Omega_a = 0$ Equations 6.47 and 6.48 give

$$Ta_{m,cr} = \sqrt{1697} = 41.19 \tag{6.51}$$

where $Ta_{m,cr}$ is the critical Taylor number based on the mean annulus radius and the corresponding Taylor number based on the mean annulus radius is defined by

$$Ta_m = \frac{\Omega r_m^{0.5} (b-a)^{1.5}}{\nu} \tag{6.52}$$

The critical angular velocity for this case is given by

$$\Omega_{cr} = \frac{41.19\nu}{r_m^{0.5}(b-a)^{1.5}} \tag{6.53}$$

For an annulus with a finite gap,

$$\Omega_{cr} = \frac{41.19\nu F_g}{r_m^{0.5}(b-a)^{1.5}} \tag{6.54}$$

where F_g is a geometrical factor defined by

$$F_g = \frac{\pi^2}{41.19\sqrt{\mathrm{S}}} \left(1 - \frac{b-a}{2r_m}\right)^{-1} \tag{6.55}$$

and S is given in an alternative form by

$$\mathrm{S} = 0.0571\left(1-0.652\frac{(b-a)/r_m}{1-(b-a)/2r_m}\right) + 0.00056\left(1-0.652\frac{(b-a)/r_m}{1-(b-a)/2r_m}\right)^{-1} \tag{6.56}$$

The wavelength for the instability is approximately

$$\lambda = 2(b-a) \tag{6.57}$$

The instability criterion developed by Taylor agrees very well with experimental data such as Schultz-Grunow (1963), Donnelly (1958), Donnelly and Fultz (1960), Donnelly and Simon (1960) and Donnelly and Schwarz (1965). The critical Taylor number and stability criterion for a wide range of radius ratios and angular velocity ratios have been widely studied and are reviewed in Andereck and Hayot (1992). Data for the resulting critical Taylor number for some of these studies are summarized in Table 6.1.

TABLE 6.1 Critical Taylor number as a function of radius ratio and angular velocity ratio. * Experimental. (Data summarized from Moalem and Cohen, 1991; Di Prima and Swinney, 1981)

a/b	Ω_b/Ω_a	$2\pi(b\text{-}a)/\lambda$	$Ta_{m,cr}$	Reference
1	–	3.12	41.18	Walowit et al. (1964)
0.975	0	3.13	41.79	Roberts (1965)
0.9625	0	3.13	42.09	Roberts (1965)
0.95	0	3.13	42.44	Roberts (1965)
0.95	−3 to 0.85	3.14	42.44	Sparrow et al. (1964)
0.95	−0.25 to 0.9025	3.12	42.45	Walowit et al. (1964)
0.925	0	3.13	43.13	Roberts (1965)
0.9	0	3.13	43.87	Roberts (1965)
0.9	−0.25 to 0.81	3.13	43.88	Walowit et al. (1964)
0.8975	0	3.13	44.66	Roberts (1965)
0.85	0	3.13	45.50	Roberts (1965)
0.80	−0.25 to 0.64	3.13	47.37	Walowit et al. (1964)
0.75	0	3.14	49.52	Roberts (1965)
0.75	−2 to 0.53	3.14	49.53	Sparrow et al. (1964)
0.70	−0.5 to 0.49	3.14	52.04	Walowit et al. (1964)
0.65	0	3.14	55.01	Roberts (1965)
0.60	−0.25 to 0.36	3.15	58.56	Walowit et al. (1964)
0.50	0	3.16	68.19	Roberts (1965)
0.5	−1.5 to 0.235	3.16	68.19	Sparrow et al. (1964)
0.5	−0.5 to 0.25	3.16	68.18	Walowit et al. (1964)
0.40	−0.25 to 0.16	3.17	83.64	Walowit et al. (1964)
0.36	0	3.19	92.72	Roberts (1965)
0.35	−0.85 to 0.116	3.21	95.38	Sparrow et al. (1964)
0.30	−0.125 to 0.09	3.20	118.89	Walowit et al. (1964)
0.28	0	3.22	120.43	Roberts (1965)
0.25	0 to 0.06	3.24	136.40	Sparrow et al. (1964)

0.25		3.33	122.91	Sparrow et al. (1964)
0.20	0	3.25	176.26	Roberts (1965)
0.20	−0.03 to 0.04	3.23	176.33	Walowit et al. (1964)
0.15	−0.15 to 0.021	3.31	250.10	Sparrow et al. (1964)
0.10	0 to 0.01	3.36	423.48	Sparrow et al. (1964)
0.10	–	3.30	422.79	Walowit et al. (1964)
0.942	−2.89 to 0.864			Taylor (1923)*
0.880	−3.25 to 0.765			Taylor (1923)*
0.873	−3 to 0.76			Coles (1965)*
0.854	−0.41 to 0.41			Nissan et al. (1963)*
0.848	−0.68 to 0			Donnelly and Fultz (1960)*
0.763	−0.705 to 0.498			Nissan et al. (1963)*
0.743	−2.73 to 0.552			Taylor (1923)*
0.698	−0.975 to 0.435			Nissan et al. (1963)*
0.584	−0.555 to 0.294			Nissan et al. (1963)*
0.9625	−1.5 to 0.25			Donnelly and Schwarz (1965)*
0.95	−1.5 to 0.25			Donnelly and Schwarz (1965)*
0.925	0			Lewis (1927)*
0.9	0			Lewis (1927)*
0.875	0			Lewis (1927)*
0.85	0			Lewis (1927)*
0.5	0			Lewis (1927)*

Example 6.7.

An annulus has inner and outer radii of 0.15 m and 0.16 m, respectively. If the annulus is filled completely with a liquid with a viscosity of 0.02 Pa s and density of 890 kg/m^3, determine the value of angular velocity at which the onset of Taylor vortices is likely to occur.

Solution

The mean radius is

$$r_m = \frac{0.15 + 0.16}{2} = 0.155\ m$$

The annular gap, $a - b$, is 0.01 m. As this is small in comparison to the mean radius, the small gap approximation can be applied.

$$\nu = \frac{\mu}{\rho} = 2.25 \times 10^{-5}$$

From Equation 6.53,

$$\Omega_{cr} = \frac{41.19\nu}{r_m^{0.5}(b-a)^{1.5}} = \frac{41.19 \times 2.25 \times 10^{-5}}{\sqrt{0.155}(0.01)^{1.5}} = 2.35\ \text{rad/s}$$

For an annulus with inner cylinder rotation, further flow regimes can occur after the first transition to the regular Taylor vortex flow illustrated in Figures 6.11 and 6.12. Extensive experimental investigations by Coles (1965), Schwarz, Springnett, and Donnelly (1964), and Snyder (1969, 1970) have revealed that many regular flow configurations can exist beyond the first transition to Taylor vortex flow; these flow configurations are generally called wavy vortex flow. These wavy vortex flow configurations are characterized by a pattern of traveling waves, which are periodic in the circumferential direction and appear just above the critical Taylor number. The transition to wavy vortex flow is not unique and is subject to strong hysteresis. As the rotational Reynolds number is further increased, experimental studies by Gollub and Swinney (1975) and Fenstermacher, Swinney, and Gollub (1979) have shown that at the onset of wavy vortex flow the velocity spectra contains a single fundamental frequency that corresponds to the traveling circumferential waves. As the rotational Reynolds number is increased, a second fundamental frequency appears at $Re_{\phi m}/Re_{\phi m,critical} = 19.3$. This second frequency has been identified as a modulation of the waves. In addition to the spectral components, a broad band characterizing weakly turbulent flow is found at $Re_{\phi m}/Re_{\phi m,critical} \approx 12$. The transition from Taylor vortex flow to wavy spiral flow has been explored numerically by Hoffmann et al. (2009).

Taylor vortex flow theory can be applied to a number of applications. Hendriks (2010) reports on the interaction between disc boundary layer flow and Taylor vortex flows in disc drives and the resultant flow-induced vibrations.

Bilgen and Boulos (1973) give the following equation for the moment coefficient for an annulus with inner cylinder rotation with no axial pressure gradient for transitional flow.

$$C_{mc} = 2\left(\frac{b-a}{a}\right)^{0.3} \mathrm{Re}_{\phi m}^{-0.6} \tag{6.58}$$

for

$$\frac{b-a}{a} > 0.07 \tag{6.59}$$

and

$$64 < \mathrm{Re}_{\phi \mathrm{m}} < 500 \tag{6.60}$$

For turbulent flow, Bilgen and Boulos (1973) give the following two equations for the moment coefficient for an annulus with inner cylinder rotation with no axial pressure gradient.

$$C_{mc} = 1.03\left(\frac{b-a}{a}\right)^{0.3} \mathrm{Re}_{\phi \mathrm{m}}^{-0.5} \tag{6.61}$$

for

$$\mathrm{Re}_{\phi \mathrm{m}} \leq 1 \times 10^4 \tag{6.62}$$

$$C_{mc} = 0.065\left(\frac{b-a}{a}\right)^{0.3} \mathrm{Re}_{\phi \mathrm{m}}^{-0.2} \tag{6.63}$$

for

$$\mathrm{Re}_{\phi \mathrm{m}} > 1 \times 10^4 \tag{6.64}$$

Example 6.8.

Determine the power required to overcome frictional drag for a 200-mm-long shaft with a diameter of 100 mm rotating in an annulus with an outer diameter of 120 mm. The rotational speed of the inner shaft is 10,000 rpm. The annulus is filled with air with a density and viscosity of 4 kg/m^3 and 3×10^{-5} Pa s, respectively. Compare the figure for the frictional drag to that of the power required to overcome equivalent cylindrical shaft also spinning at 10,000 rpm in Example 6.1.

Solution

From Equation 6.29,

$$\mathrm{Re}_{\phi m} = \frac{\rho \Omega a(b-a)}{\mu} = \frac{4 \times 1047 \times 0.05 \times 0.01}{3 \times 10^{-5}} = 69800$$

As the rotational Reynolds number is greater than 10,000, then from Equation 6.63,

$$C_{mc} = 0.065\left(\frac{b-a}{a}\right)^{0.3} \mathrm{Re}_{\phi m}^{-0.2} = 0.065\left(\frac{0.01}{0.05}\right)^{0.3} (69800)^{-0.2} = 4.310 \times 10^{-3}$$

The power required to overcome frictional drag, from Equation 6.8, is

$$\text{Power} = 0.5\pi\rho\Omega^3 a^4 L C_{mc} = 0.5\pi \times 4 \times 1047^3 \times 0.05^4 \times 0.2 \times 4.31 \times 10^{-3} = 38.85\,\mathrm{W}$$

The power required to overcome drag for the rotating shaft located in the annulus is about 40% of that of the rotating cylinder of Example 6.1.

Experiments using hot wire anemometry and flow visualization, for the case of a throughflow of superposed axial air with inner cylinder by Kaye and Elgar (1958) revealed the existence of four modes of flow:

- purely laminar flow
- laminar flow with Taylor vortices
- turbulent flow with vortices
- turbulent flow

Kaye and Elgar's (1958) tests were performed using an annulus with inner and outer radii of 34.9 mm and 47.5 mm, respectively, at axial Reynolds numbers up to 2000 and rotational Reynolds numbers up to 3000. A schematic of the resulting flow regimes as a function of the axial and rotational Reynolds numbers is given in Figure 6.13.

The Rayleigh inviscid criterion for rotational instability remains valid for the case of an annulus with axial throughflow and a fully developed tangential velocity as shown by Chandrasekhar (1960a). Using linear stability theory to predict the onset of instability for the case an annulus with a narrow gap, $a/b \rightarrow 1$, Chandrasekhar (1960b) and Di-Prima (1960) found that the onset of instability increased monotonically with the axial velocity. The critical Taylor number for the case of inner cylinder rotation with axial throughflow is given by

$$Ta_{cr}^2 = Ta_{cr,\mathrm{Re}_{z=0}}^2 + 26.5\mathrm{Re}_z^2 \tag{6.65}$$

where the axial Reynolds number Re_z is given by

$$Re_z = \frac{\rho u_z (b-a)}{\mu} \tag{6.66}$$

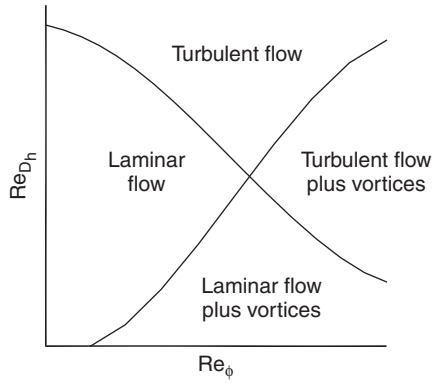

FIGURE 6.13 Schematic representation of the four modes of flow in an annulus with axial throughflow and inner cylinder rotation (after Kaye and Elgar, 1958).

Schwarz et al. (1964) gave the following relationship for the critical Taylor number for an annulus with inner cylinder rotation and axial throughflow based on their experimental measurements, for a narrow gap annulus with $Re_z < 25$.

$$Ta_{cr}^2 = \frac{2(a/b)^2(b-a)^4}{1-(a/b)^2}\frac{\Omega^2}{\nu^2} \tag{6.67}$$

6.5. JOURNAL BEARINGS

The term *bearing* typically refers to contacting surfaces through which a load is transmitted. Bearings may roll or slide or do both simultaneously. The range of bearing types available is extensive, although they can be broadly split into two categories: sliding bearings (see Figure 6.14), where the motion is facilitated by a thin layer or film of lubricant, and rolling element bearings, where the motion is aided by a combination of rolling motion and lubrication. Lubrication is often required in a bearing to reduce friction between surfaces and to remove heat. Here consideration will be limited to the fluid flow associated with one particular type of sliding bearings, rotating journal bearings. An introduction to rolling element bearings is given in Childs (2004).

The term *sliding bearing* refers to bearings where two surfaces move relative to each other without the benefit of rolling contact. The two surfaces slide over each other, and this motion can be facilitated by means of a lubricant that gets squeezed by the motion of the components and can under certain conditions generate sufficient pressure to separate the surfaces, thereby reducing frictional contact and wear. A typical application of sliding bearings is to allow rotation of a load-carrying shaft. The portion of the shaft at the bearing is referred to as the journal, and the stationary part, which supports the load, is called the bearing (see Figure 6.15). For this reason, sliding bearings are

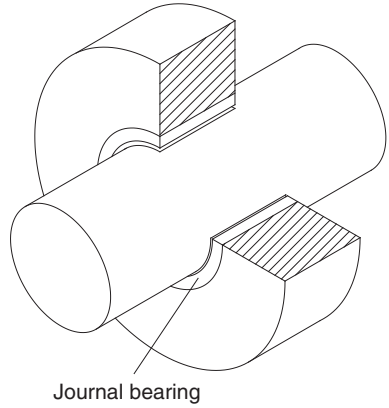

FIGURE 6.14 A journal bearing.

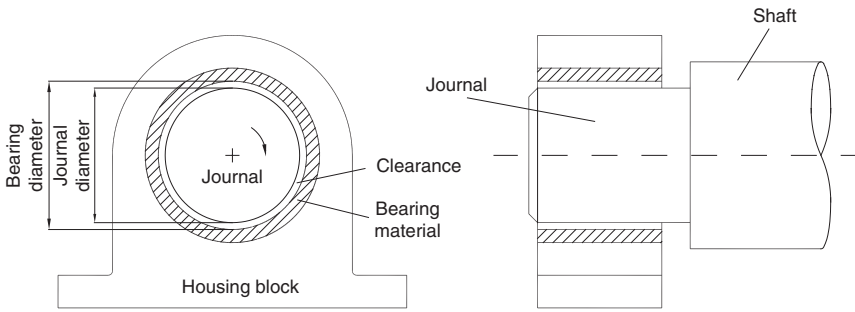

FIGURE 6.15 A plain surface, sliding, or journal bearing.

often collectively referred to as journal bearings, although this term ignores the existence of sliding bearings that support linear translation of components. Another common term is *plain surface bearings.* This section is concerned principally with bearings for rotary motion, and the terms *journal* and *sliding bearing* are used interchangeably.

There are three principal regimes of lubrication for sliding bearings:

1. boundary lubrication
2. mixed film lubrication
3. full film lubrication

Boundary lubrication typically occurs at low relative velocities between the journal and the bearing surfaces and is characterized by actual physical contact. The surfaces, even if ground to a very low value of surface roughness, will still consist of a series of peaks and troughs as illustrated schematically in Figure 6.16. Although some lubricant may be present, the pressures generated within it are not significant, and the relative motion of the surfaces brings the corresponding peaks periodically into contact. Mixed film lubrication occurs when the relative motion between the surfaces is sufficient to generate high enough

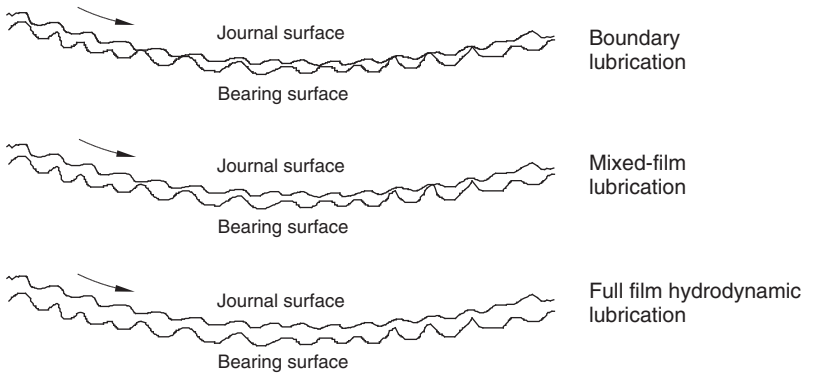

FIGURE 6.16 Schematic representation of the surface roughness for sliding bearings and the relative position depending on the type of lubrication occurring.

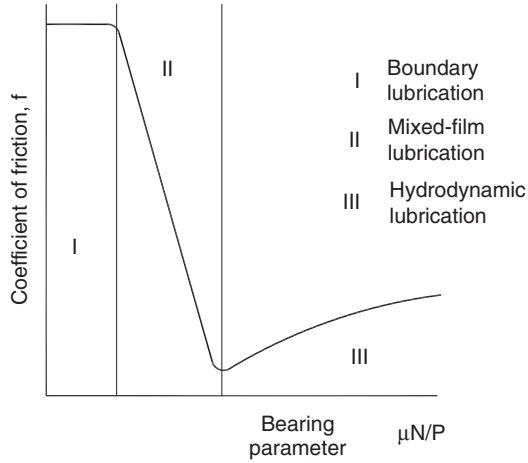

FIGURE 6.17 Schematic representation of the variation of bearing performance with lubrication.

pressures in the lubricant film, which can partially separate the surfaces for periods of time. There is still contact in places around the circumference between the two components. Full film lubrication occurs at higher relative velocities. Here the motion of the surface generates high pressures in the lubricant, which separate the two components and the journal can "ride" on a wedge of fluid. All of these types of lubrication can be encountered in a bearing without external pressure of the bearing. If lubricant under high enough pressure is supplied to the bearing to separate the two surfaces, it is called a hydrostatic bearing.

The performance of a sliding bearing differs markedly, depending on which type of lubrication is physically occurring. This is illustrated in Figure 6.17, which shows the characteristic variation of the coefficient of friction with a group of variables called the bearing parameter, which is defined by

$$\frac{\mu N}{P} \tag{6.68}$$

where

μ = viscosity of lubricant (Pa s)
N = speed (for this definition normally given in rpm)
P = load capacity (N/m^2) given in Equation 6.69

$$P = \frac{W}{LD} \tag{6.69}$$

where

W = applied load (N)
L = bearing length (m)
D = journal diameter (m)

The bearing parameter, $\mu N/P$, groups several of the bearing design variables into one number. Normally, of course, a low coefficient of friction is desirable in order

to reduce the power lost in the overcoming friction. In general, boundary lubrication is used for slow speed applications where the surface speed is less than approximately 1.5 m/s. Mixed film lubrication is rarely used because it is difficult to quantify the actual value of the coefficient of friction (note the steep gradient in Figure 6.17 for this zone). The design of boundary-lubricated bearings is outlined in Section 6.5.1, and full film hydrodynamic bearings are described in Section 6.5.2.

As can be seen from Figure 6.17, bearing performance is dependent on the type of lubrication occurring and the viscosity of the lubricant. The viscosity is a measure of a fluid's resistance to shear. Lubricants can be solid, liquid, or gaseous, although the most commonly known are oils and greases. The principal classes of liquid lubricants are mineral oils and synthetic oils. Their viscosity is highly dependent on temperature and pressure as indicated for the case of temperature in Figure 6.18. They are typically solid at –35 °C, thin as paraffin at 100 °C, and burn above 240 °C. Many additives are used to affect their performance. For example, EP (extreme pressure) additives add fatty acids and other compounds to the oil, which attack the metal surfaces to form "contaminant" layers, which protect the surfaces and reduce friction even when the oil film is squeezed out by high-contact loads. Greases are oils mixed with soaps to form a thicker lubricant that can be retained on surfaces.

The viscosity variation with temperature of oils has been standardized, and oils are available with a class number—for example, SAE 10, SAE 20, SAE 30,

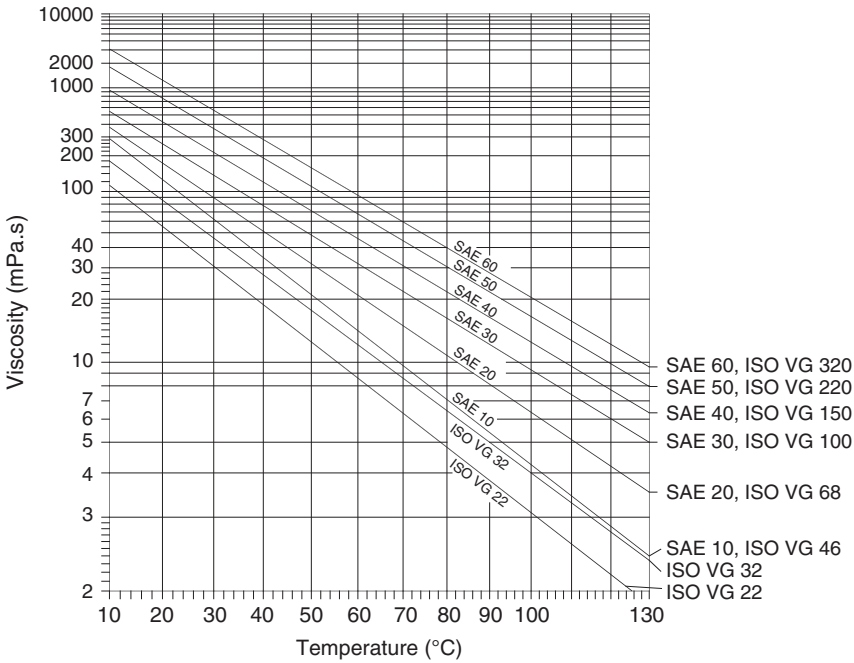

FIGURE 6.18 Variation of absolute viscosity with temperature for various lubricants.

SAE 40, SAE 5W, and SAE 10W. The Society of Automotive Engineers developed this identification system in order to class oils for general-purpose use and winter use, the "W" signifying the latter. The lower the numerical value, the thinner or less viscous the oil. Multigrade oil (e.g., SAE 10W/40) is formulated to meet the viscosity requirements of two oils, giving some of the benefits of the constituent parts. An equivalent identification system is also available from the International Organization for Standardization (ISO 3448).

6.5.1 Boundary-Lubricated Bearings

As described in Section 6.5, the journal and bearing surfaces in a boundary lubricated bearing are in direct contact in places. These bearings are typically used for very-low-speed applications such as bushes and linkages where their simplicity and compact nature are advantageous. Examples include shafts for gear wheels in electric tools, lawnmower wheels, garden hand tools such as shears, ratchet wrenches, and domestic and automotive door hinges incorporating the journal as a solid pin riding inside a cylindrical outer member.

General considerations in the design of a boundary lubricated bearing are:

- the coefficient of friction (both static and dynamic)
- the load capacity
- the relative velocity between the stationary and moving components
- the operating temperature
- wear limitations
- the production capability

A useful measure in the design of boundary-lubricated bearings is the PV factor (load capacity $\times$ peripheral speed), which indicates the ability of the bearing material to accommodate the frictional energy generated in the bearing. At the limiting PV value the temperature will be unstable, and failure will occur rapidly. A practical value for PV is half the limiting PV value. Values for PV depend on the material combinations concerned and typically vary between 0.035 in the case of thermoplastic with filler to 1.75 for PTFE with filler, bonded to steel backing. The preliminary design of a boundary lubricated bearing essentially consists of setting the bearing proportions, its length and its diameter, and selecting the bearing material such that an acceptable PV value is obtained. This approach is set out as a step-by-step procedure as follows.

1. Determine the speed of rotation of the bearing and the load to be supported.
2. Set the bearing proportions. Common practice is to set the length to diameter ratio between 0.5 and 1.5. If the diameter D is known as an initial trial, set L equal to D.
3. Calculate the load capacity, $P = W/(LD)$.
4. Determine the maximum tangential speed of the journal.
5. Calculate the PV factor ($P \times u_{\phi}$).
6. Multiply the PV value obtained by a factor of safety of 2.

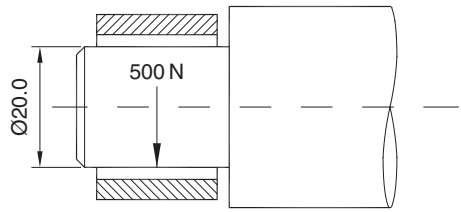

FIGURE 6.19 Boundary lubricated bearing design example.

7. Interrogate manufacturer's data or the limited example data in Table 6.2 to identify an appropriate bearing material with a value for *PV* factor greater than that obtained in (6).

Example 6.9.

A bearing is to be designed to carry a radial load of 500 N for a shaft of diameter 20 mm running at a speed of 100 rpm (see Figure 6.19). Calculate the *PV* factor, and by comparison with the available materials listed in Table 6.2 determine a suitable bearing material.

Solution

The primary data are $W = 500$ N, $D = 20$ mm, and $N = 100$ rpm.

Use $L/D = 1$ as an initial suggestion for the length to diameter ratio for the bearing. $L = 20$ mm.

Calculating the load capacity, P

$$P = \frac{W}{LD} = \frac{500}{0.02 \times 0.02} = 1.25 \text{ MN/m}^2$$

$$u_\phi = \Omega a = \left(\frac{2\pi}{60}\right) N \frac{D}{2} = 0.1047 \times 100 \times \frac{0.02}{2} = 0.1047 \text{ m/s}$$

$$PV \approx 0.13 \quad (\text{MN/m}^2)(\text{m/s})$$

Multiplying this by a safety of factor of 2 gives a *PV* factor of 0.26 (MN/m s)

A material with PV factor greater than this, such as filled PTFE (limiting PV factor up to 0.35), or PTFE with filler bonded to a steel backing (limiting PV factor up to 1.75), would give acceptable performance.

6.5.2 Design of Full Film Hydrodynamic Bearings

In a full film hydrodynamic bearing, the load on the bearing is supported on a continuous film of lubricant so that no contact between the bearing and the rotating journal occurs. The motion of the journal inside the bearing creates the

TABLE 6.2 Characteristics of some rubbing materials. Reproduced courtesy of Neale (1995)

MATERIAL	MAXIMUM LOAD CAPACITY P (MN/m^2)	LIMITING PV FACTOR (MN/m s)	MAXIMUM OPERATING TEMPERATURE (°C)	COEFFICIENT OF FRICTION	COEFFICIENT OF EXPANSION ($\times 10^{-6}/^{O}C$)	COMMENTS	TYPICAL APPLICATION
Carbon/ graphite	1.4 – 2	0.11	350–500	0.1–0.25 dry	2.5–5.0	For continuous dry operation	Food and textile machinery
Carbon/ graphite with metal	3.4	0.145	130–350	0.1–0.35 dry	4.2–5		
Graphite impregnated metal	70	0.28–0.35	350–600	0.1–0.15 dry	12–13		
Graphite/ thermo-setting resin	2	0.35	250	0.13–0.5 dry	3.5–5	Suitable for sea water operation	
Reinforced thermo-setting plastics	35	0.35	200	0.1–0.4 dry	25–80		Roll-neck bearings
Thermo-plastic material without filler	10	0.035	100	0.1–0.45 dry	100		Bushes and thrust washers
Thermo-plastic with filler or metal backed	10–14	0.035–0.11	100	0.15–0.4 dry	80–100		Bushes and thrust washers

(*Continued*)

Table 6.2 (*Continued*)

MATERIAL	MAXIMUM LOAD CAPACITY P (MN/m^2)	LIMITING PV FACTOR (MN/m s)	MAXIMUM OPERATING TEMPERATURE (°C)	COEFFICIENT OF FRICTION	COEFFICIENT OF EXPANSION ($\times 10^{-6}/^{O}C$)	COMMENTS	TYPICAL APPLICATION
Thermo-plastic material with filler bonded to metal back	140	0.35	105	0.2–0.35 dry	27	With initial lubrication only	For conditions of intermittent operation or boundary lubrication e.g. ball joints, suspension, steering
Filled PTFE	7	up to 0.35	250	0.05–0.35 dry	60–80	Glass, mica, bronze, graphite	For dry operations where low friction and wear required
PTFE with filler, bonded to steel backing	140	up to 1.75	280	0.05–0.3 dry	20	Sintered bronze bonded to steel backing impregnated with PTFE/lead	Aircraft controls, linkages, gearbox, clutch, conveyors, bridges
Woven PTFE reinforced and bonded to metal backing	420	up to 1.6	250	0.03–0.3	–	Reinforcement may be interwoven glass fibre or rayon	Aircraft and engine controls, linkages, engine mountings, bridge bearings

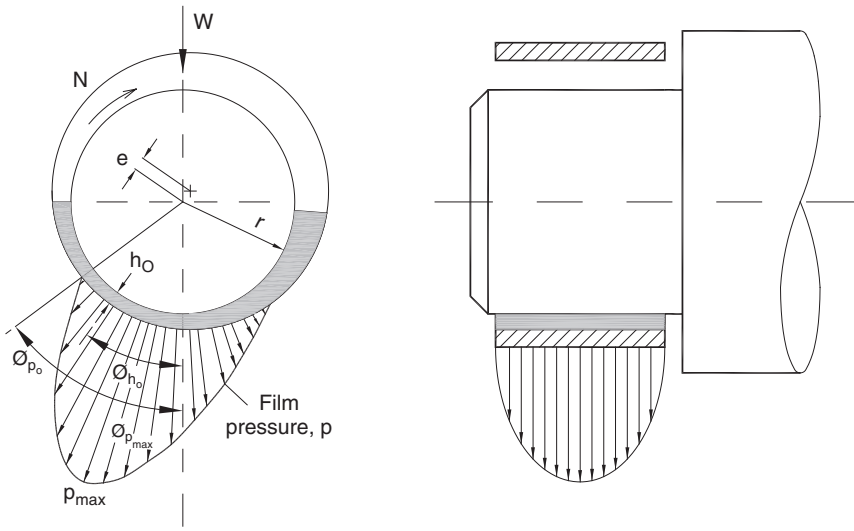

FIGURE 6.20 Motion of the journal generates pressure in the lubricant separating the two surfaces. Beyond h_o, the minimum film thickness, the pressure terms go negative and the film is ruptured.

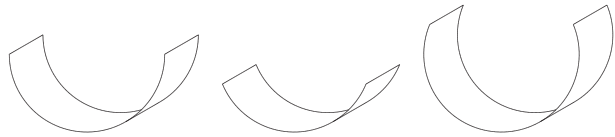

FIGURE 6.21 Partial surface journal bearings.

necessary pressure to support the load (Figure 6.20). Hydrodynamic bearings are commonly found in internal combustion engines for supporting the crankshaft and in turbocharger applications. Hydrodynamic bearings can consist of a full circumferential surface or a partial surface around the journal (Figure 6.21).

Bearing design involves a significant number of often conflicting parameters, with improvement in one feature resulting in deterioration in another. One approach to designing a bearing system would be to assign attribute points to each aspect of the design and undertake an optimization exercise. This, however, would be time consuming if the software was not already in a developed state and would not necessarily produce an optimum result due to inadequacies in modeling and incorrect assignment of attribute weightings. An alternative approach, which is sensible as a starting point and outlined here, is to develop one or a number of feasible designs and use judgments to select the best, or combine the best features of the proposed designs.

The design procedure for a journal bearing, recommended here as a starting point, includes the specification of the journal radius a, the radial clearance c, the axial length of the bearing surface, L, the type of lubricant and its viscosity, μ, the journal speed, N, and the load, W. Values for the speed, the load, and possibly

the journal radius are usually specified by the machine requirements and stress and deflection considerations. As such, journal bearing design consists of the determination of the radial clearance, the bearing length, and the lubricant viscosity. The design process for a journal bearing is usually iterative. Trial values for the clearance, the length and the viscosity are chosen, various performance criteria calculated, and the process repeated until a satisfactory or optimized design is achieved. Criteria for optimization may be minimizing of the frictional loss, minimizing the lubricant temperature rise, minimizing the lubricant supply, maximizing the load capability, and minimizing production costs.

The clearance between the journal and the bearing depends on the nominal diameter of the journal, the precision of the machine, surface roughness, and thermal expansion considerations. An overall guideline is for the radial clearance, c, to be in the range $0.001a < c < 0.002a$, where a is the nominal bearing radius ($0.001D < 2c < 0.002$D). Figure 6.22 shows values for the recommended diametral clearance ($2 \times c$) as a function of the journal diameter and rotational speed for steadily loaded bearings.

For a given combination of a, c, L, μ, N, and W, the performance of a journal bearing can be calculated. This requires determining the pressure distribution in the bearing, the minimum film thickness h_o, the location of the minimum film

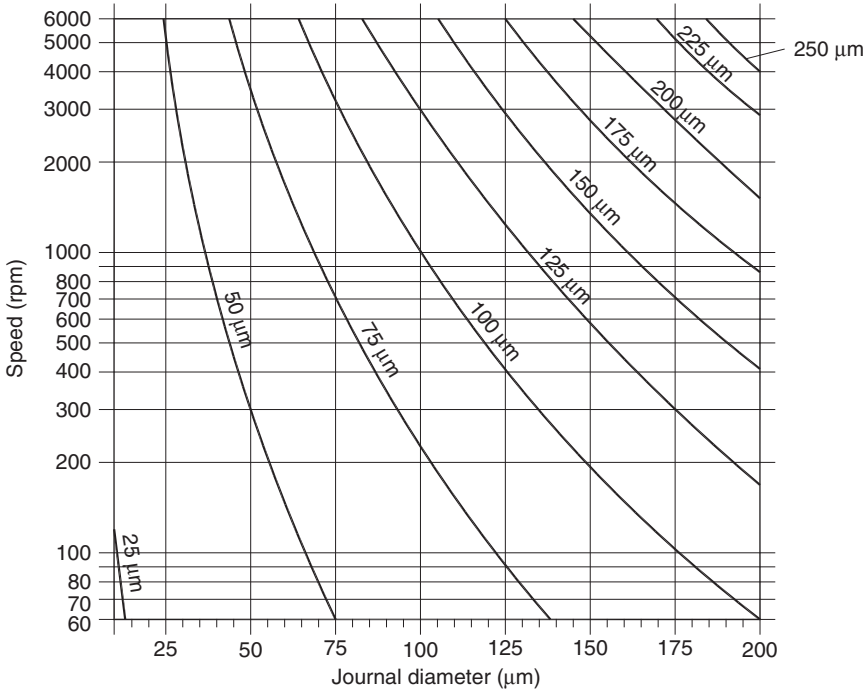

FIGURE 6.22 Minimum recommended values for the diametral clearance ($2 \times c$) for steadily loaded journal bearings (reproduced from Welsh, 1983).

thickness $\phi_{p_{\max}}$, the coefficient of friction f, the lubricant flow Q, the maximum film pressure p_{max}, and the temperature rise ΔT of the lubricant.

The pressure distribution in a journal bearing (see Figure 6.20) can be determined by solving the relevant form of the Navier-Stokes fluid flow equations, which in the reduced form for journal bearings is called the Reynolds equation and was first derived by Reynolds (1886) and further developed by Harrison (1913) to include the effects of compressibility. Here the derivation of the general Reynolds equation is developed following the general outline given by Hamrock (1994).

The Navier-Stokes equations in a Cartesian coordinate system, for compressible flow assuming constant viscosity, are given by Equations 2.46–2.48 and repeated here for convenience, Equations 6.70–6.72. Here x is taken as the coordinate in the direction of sliding, y is the coordinate in the direction of side leakage and z is the coordinate across the lubricant film.

$$\rho\left(\frac{\partial u_x}{\partial t}+u_x\frac{\partial u_x}{\partial x}+u_y\frac{\partial u_x}{\partial y}+u_z\frac{\partial u_x}{\partial z}\right)=-\frac{\partial p}{\partial x}+\mu\left(\frac{\partial^2 u_x}{\partial x^2}+\frac{\partial^2 u_x}{\partial y^2}+\frac{\partial^2 u_x}{\partial z^2}\right)+\frac{\mu}{3}\frac{\partial}{\partial x}\left(\frac{\partial u_x}{\partial x}+\frac{\partial u_y}{\partial y}+\frac{\partial u_z}{\partial z}\right)+F_x \tag{6.70}$$

$$\rho\left(\frac{\partial u_y}{\partial t}+u_x\frac{\partial u_y}{\partial x}+u_y\frac{\partial u_y}{\partial y}+u_z\frac{\partial u_y}{\partial z}\right)=-\frac{\partial p}{\partial y}+\mu\left(\frac{\partial^2 u_y}{\partial x^2}+\frac{\partial^2 u_y}{\partial y^2}+\frac{\partial^2 u_y}{\partial z^2}\right)+\frac{\mu}{3}\frac{\partial}{\partial y}\left(\frac{\partial u_x}{\partial x}+\frac{\partial u_y}{\partial y}+\frac{\partial u_z}{\partial z}\right)+F_y \tag{6.71}$$

$$\rho\left(\frac{\partial u_z}{\partial t}+u_x\frac{\partial u_z}{\partial x}+u_y\frac{\partial u_z}{\partial y}+u_z\frac{\partial u_z}{\partial z}\right)=-\frac{\partial p}{\partial z}+\mu\left(\frac{\partial^2 u_z}{\partial x^2}+\frac{\partial^2 u_z}{\partial y^2}+\frac{\partial^2 u_z}{\partial z^2}\right)+\frac{\mu}{3}\frac{\partial}{\partial z}\left(\frac{\partial u_x}{\partial x}+\frac{\partial u_y}{\partial y}+\frac{\partial u_z}{\partial z}\right)+F_z \tag{6.72}$$

If the density is assumed constant, then the dilation, Equation 6.73, is zero.

$$\frac{\partial u_x}{\partial x}+\frac{\partial u_y}{\partial y}+\frac{\partial u_z}{\partial z}=0 \tag{6.73}$$

The Navier-Stokes equations for constant density and constant viscosity reduce to

$$\rho\left(\frac{\partial u_x}{\partial t}+u_x\frac{\partial u_x}{\partial x}+u_y\frac{\partial u_x}{\partial y}+u_z\frac{\partial u_x}{\partial z}\right)=-\frac{\partial p}{\partial x}+\mu\left(\frac{\partial^2 u_x}{\partial x^2}+\frac{\partial^2 u_x}{\partial y^2}+\frac{\partial^2 u_x}{\partial z^2}\right)+F_x \tag{6.74}$$

$$\rho\left(\frac{\partial u_y}{\partial t}+u_x\frac{\partial u_y}{\partial x}+u_y\frac{\partial u_y}{\partial y}+u_z\frac{\partial u_y}{\partial z}\right)=-\frac{\partial p}{\partial y}+\mu\left(\frac{\partial^2 u_y}{\partial x^2}+\frac{\partial^2 u_y}{\partial y^2}+\frac{\partial^2 u_y}{\partial z^2}\right)+F_y \tag{6.75}$$

$$\rho\left(\frac{\partial u_z}{\partial t}+u_x\frac{\partial u_z}{\partial x}+u_y\frac{\partial u_z}{\partial y}+u_z\frac{\partial u_z}{\partial z}\right)=-\frac{\partial p}{\partial z}+\mu\left(\frac{\partial^2 u_z}{\partial x^2}+\frac{\partial^2 u_z}{\partial y^2}+\frac{\partial^2 u_z}{\partial z^2}\right)+F_z \tag{6.76}$$

For conditions known as slow viscous motion, where pressure and viscous terms predominate, simplifications are possible for the Navier-Stokes equations, making their solution more amenable to analytical and numerical techniques.

The Navier-Stokes equations can be nondimensionalized to enable a generalized solution, using the same procedure as described in Section 2.6. Here the process is repeated to give dimensionless groups of specific relevance to journal bearings, using the characteristic parameters given in Equations 6.77–6.86.

$$x_* = \frac{x}{l_o} \tag{6.77}$$

where l_o is a characteristic length in the x direction.

$$y_* = \frac{y}{b_o} \tag{6.78}$$

where b_o is a characteristic length in the y direction.

$$z_* = \frac{z}{h_o} \tag{6.79}$$

where h_o is a characteristic length in the z direction.

$$t_* = \frac{t}{t_o} \tag{6.80}$$

where t_o is a characteristic time.

$$u_{x*} = \frac{u_x}{u_{x,o}} \tag{6.81}$$

where $u_{x,o}$ is a characteristic velocity in the x direction.

$$u_{y*} = \frac{u_y}{u_{y,o}} \tag{6.82}$$

where $u_{y,o}$ is a characteristic velocity in the y direction.

$$u_{z*} = \frac{u_z}{u_{z,o}} \tag{6.83}$$

where $u_{z,o}$ is a characteristic velocity in the z direction.

$$\rho_* = \frac{\rho}{\rho_o} \tag{6.84}$$

where ρ_o is a characteristic density.

$$\mu_* = \frac{\mu}{\mu_o} \tag{6.85}$$

where μ_o is a characteristic viscosity.

$$p_* = \frac{h_o^2 p}{\mu_o u_{x,o} l_o} \tag{6.86}$$

Substitution of the above dimensionless parameters, Equations 6.77–6.86 in Equation 6.70, gives

$$\begin{aligned}
&\frac{l_o}{u_{x,o}t_o}\frac{\partial u_{x*}}{\partial t_*} + u_{x*}\frac{\partial u_{x*}}{\partial x_*} + \frac{l_o u_{y,o}}{b_o u_{x,o}} u_{y*}\frac{\partial u_{x*}}{\partial y_*} + \frac{l_o u_{z,o}}{h_o u_{x,o}} u_{z*}\frac{\partial u_{x*}}{\partial z_*} = \frac{l_o g}{u_{x,o}^2} \\
&-\frac{\mu_o}{\rho_o u_{x,o} l_o}\left(\frac{l_o}{h_o}\right)^2 \frac{1}{\rho_*}\frac{\partial p_*}{\partial x_*} - \frac{2}{3}\frac{\mu_o}{\rho_o u_{x,o} l_o}\frac{1}{\rho_*}\frac{\partial}{\partial x_*}\left[\mu_*\left(\frac{\partial u_{x*}}{\partial x_*} + \frac{u_{y,o} l_o}{u_{x,o} b_o}\frac{\partial u_{y*}}{\partial y_*} + \frac{u_{z,o} l_o}{u_{x,o} h_o}\frac{\partial u_{z*}}{\partial z_*}\right)\right] \\
&+\frac{2\mu_o}{\rho_o u_{x,o} l_o}\frac{1}{\rho_*}\frac{\partial}{\partial x_*}\left(\mu_*\frac{\partial u_{x*}}{\partial x_*}\right) + \frac{\mu_o}{\rho_o u_{x,o} l_o}\left(\frac{l_o}{b_o}\right)^2 \frac{1}{\rho_*}\frac{\partial}{\partial y_*}\left[\mu_*\left(\frac{\partial u_{x*}}{\partial y_*} + \frac{u_{y,o} b_o}{u_{x,o} l_o}\frac{\partial u_{y*}}{\partial x_*}\right)\right] \\
&+\frac{\mu_o}{\rho_o u_{x,o} l_o}\left(\frac{l_o}{h_o}\right)^2 \frac{1}{\rho_*}\frac{\partial}{\partial z_*}\left[\mu_*\left(\frac{\partial u_{x*}}{\partial z_*} + \frac{u_{z,o} h_o}{u_{x,o} l_o}\frac{\partial u_{z*}}{\partial x_*}\right)\right]
\end{aligned} \tag{6.87}$$

The relative importance of inertia and viscous forces can be determined by examining the value of the Reynolds number

$$\mathrm{Re} = \frac{\rho_o u_{x,o} l_o}{\mu_o} \tag{6.88}$$

The inverse of the Reynolds number occurs throughout Equation 6.87.

In fluid film lubrication, because of the dominance of the viscous term $\partial^2 u_{x*}/\partial^2 z_*$, a modified form of the Reynolds number is used, defined for the x component of velocity by

$$\mathrm{Re}_x = \frac{\rho_o u_{x,o} h_o^2}{\mu_o l_o} \tag{6.89}$$

and similarly for the y and z directions

$$\mathrm{Re}_y = \frac{\rho_o u_{y,o} h_o^2}{\mu_o b_o} \tag{6.90}$$

$$\mathrm{Re}_z = \frac{\rho_o u_{z,o} h_o}{\mu_o} \tag{6.91}$$

The squeeze number is defined by

$$\sigma_s = \frac{\rho_o h_o^2}{\mu_o t_o} \tag{6.92}$$

Typically, in hydrodynamically lubricated journal bearings, viscous forces are much greater than inertia forces, and a typical Reynolds number, using Equation 6.89, might be of the order of 1×10^{-4}.

Substitution of the Reynolds and squeeze numbers into Equation 6.87 gives

$$\begin{aligned}
&\sigma_s \frac{\partial u_{x*}}{\partial t_*} + \mathrm{Re}_x u_{x*} \frac{\partial u_{x*}}{\partial x_*} + \mathrm{Re}_y u_{y*} \frac{\partial u_{x*}}{\partial y_*} + \mathrm{Re}_z u_{z*} \frac{\partial u_{x*}}{\partial z_*} = \frac{l_o g}{u_{x,o}^2} \mathrm{Re}_x - \frac{1}{\rho_*} \frac{\partial p_*}{\partial x_*} \\
&+ \frac{1}{\rho_*} \frac{\partial}{\partial z_*} \left(\mu_* \frac{\partial u_{x*}}{\partial z_*} \right) - \frac{2}{3} \left(\frac{h_o}{l_o} \right)^2 \frac{1}{\rho_*} \frac{\partial}{\partial x_*} \left[\mu_* \left(\frac{\partial u_{x*}}{\partial x_*} + \frac{u_{y,o} l_o}{u_{x,o} b_o} \frac{\partial u_{y*}}{\partial y_*} + \frac{u_{z,o} l_o}{u_{x,o} h_o} \frac{\partial u_{z*}}{\partial z_*} \right) \right] \\
&+ \left(\frac{h_o}{b_o} \right)^2 \frac{1}{\rho_*} \frac{\partial}{\partial y_*} \left[\mu_* \left(\frac{\partial u_{x*}}{\partial y_*} + \frac{u_{y,o} b_o}{u_{x,o} l_o} \frac{\partial u_{y*}}{\partial x_*} \right) \right] + 2 \left(\frac{h_o}{l_o} \right)^2 \frac{1}{\rho_*} \frac{\partial}{\partial x_*} \left(\mu_* \frac{\partial u_{x*}}{\partial x_*} \right) \\
&+ \frac{1}{\rho_*} \frac{\partial}{\partial z_*} \left(\mu_* \frac{u_{z,o} h_o}{u_{x,o} l_o} \frac{\partial u_{z*}}{\partial x_*} \right)
\end{aligned} \tag{6.93}$$

Examination of the order of magnitude of the terms in Equation 6.93 provides an indication of the relative significance of each of these and therefore which need to considered. The inertia terms, gravity term, and $u_{z,o}/u_{x,o}$ are of order h_o/l_o. The pressure gradient term and the first viscous term are of order unity. The remaining viscous terms are of order $(h_o/l_o)^2$ or $(h_o/b_o)^2$ and therefore very small in comparison to the other terms. Neglecting terms of the order of $(h_o/l_o)^2$ and $(h_o/b_o)^2$ gives

$$\begin{aligned}
&\sigma_s \frac{\partial u_{x*}}{\partial t_*} + \mathrm{Re}_x u_{x*} \frac{\partial u_{x*}}{\partial x_*} + \mathrm{Re}_y u_{y*} \frac{\partial u_{x*}}{\partial y_*} + \mathrm{Re}_z u_{z*} \frac{\partial u_{x*}}{\partial z_*} = \frac{l_o g}{u_{x,o}^2} \mathrm{Re}_x - \frac{1}{\rho_*} \frac{\partial p_*}{\partial x_*} \\
&+ \frac{1}{\rho_*} \frac{\partial}{\partial z_*} \left(\mu_* \frac{\partial u_{x*}}{\partial z_*} \right)
\end{aligned} \tag{6.94}$$

Similarly, for the y and z components

$$\sigma_s \frac{\partial u_{y*}}{\partial t_*} + \mathrm{Re}_x u_{x*} \frac{\partial u_{y*}}{\partial x_*} + \mathrm{Re}_y u_{y*} \frac{\partial u_{y*}}{\partial y_*} + \mathrm{Re}_z u_{z*} \frac{\partial u_{y*}}{\partial z_*} = \frac{b_o g}{u_{y,o}^2} \mathrm{Re}_y - \frac{1}{\rho_*} \frac{\partial p_*}{\partial y_*} + \frac{1}{\rho_*} \frac{\partial}{\partial z_*} \left(\mu_* \frac{\partial u_{y*}}{\partial z_*} \right) \tag{6.95}$$

$$\frac{\partial p}{\partial z_*} = 0 \tag{6.96}$$

Examination of Equations 6.94–6.96 shows that the pressure is a function of x_*, y_*, and t_*,

$$p = f(x_*, y_*, t_*) \tag{6.97}$$

The continuity equation can be expressed as

$$\sigma_s \frac{\partial p_*}{\partial t_*} + \mathrm{Re}_x \frac{\partial}{\partial x_*} (\rho_* u_{x*}) + \mathrm{Re}_y \frac{\partial}{\partial y_*} (\rho_* u_{y*}) + \mathrm{Re}_z \frac{\partial}{\partial z_*} (\rho_* u_{z*}) = 0 \tag{6.98}$$

A check can be made to identify if Taylor vortices are likely to occur. If the Taylor number, Equation 6.12, is greater than approximately 41.2, then Taylor vortices may form, and laminar flow conditions may no longer hold, invalidating the use of the equations developed in this section.

The Froude number, Equation 2.142, indicates the relative importance of inertia and gravity forces. A typical Froude number for a journal bearing might be of the order of 10, providing an indication that gravity forces can be neglected in comparison with viscous forces.

The importance of pressure relative to inertia can be judged by examining the Euler number, Equation 2.143. For a typical journal bearing, the Euler number may be of the order of 100, indicating that the pressure term is much larger than the inertia term.

If in addition to neglecting terms of order $(h_o/l_o)^2$ or $(h_o/b_o)^2$, terms of the order of h_o/l_o and h_o/b_o are neglected and only terms of the order of unity are considered, the Navier-Stokes equations reduce to

$$\frac{\partial p}{\partial x} = \frac{\partial}{\partial z} \left(\mu \frac{\partial u_x}{\partial z} \right) \tag{6.99}$$

$$\frac{\partial p}{\partial y} = \frac{\partial}{\partial z} \left(\mu \frac{\partial u_y}{\partial z} \right) \tag{6.100}$$

Equation 6.97 shows that the pressure is only a function of x and y for steady-state conditions. Equations 6.99 and 6.100 can therefore be integrated directly to give general expressions for the velocity gradients as follows.

$$\frac{\partial u_x}{\partial z} = \frac{z}{\mu} \frac{\partial p}{\partial x} + \frac{A}{\mu} \tag{6.101}$$

$$\frac{\partial u_y}{\partial z} = \frac{z}{\mu}\frac{\partial p}{\partial y} + \frac{C}{\mu} \tag{6.102}$$

where A and C are constants of integration.

The temperature across the thin layer of layer lubricant in a journal bearing may vary significantly. As viscosity is highly dependent on temperature, this leads to increased complexity in obtaining a solution to Equations 6.101 and 6.102. In many fluid film applications, however, it has been found acceptable to model the viscosity of a fluid film using an average value for the viscosity across the film. With μ taken as the average value of viscosity across the fluid film, integration of Equations 6.101 and 6.102 gives the velocity components as follows.

$$u_x = \frac{z^2}{2\mu}\frac{\partial p}{\partial x} + A\frac{z}{\mu} + B \tag{6.103}$$

$$u_y = \frac{z^2}{2\mu}\frac{\partial p}{\partial y} + C\frac{z}{\mu} + D \tag{6.104}$$

where B and D are constants of integration.

If the no-slip condition is assumed at the fluid solid interface, then the boundary conditions are as follows and illustrated in Figure 6.23.

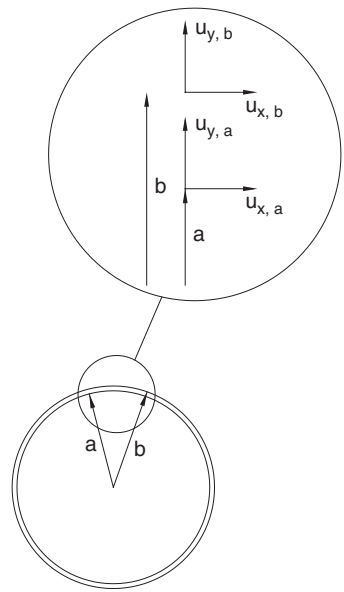

FIGURE 6.23 Journal bearing boundary conditions.

$u_x = u_{x,a}$, $u_y = u_{y,a}$ at $z = 0$
$u_x = u_{x,b}$, $u_y = u_{y,b}$ at $z = h$

Application of the boundary conditions to the equations for the velocity gradients and velocity components, Equations 6.103–6.104, gives

$$\frac{\partial u_x}{\partial z} = \frac{2z-h}{2\mu}\frac{\partial p}{\partial x} - \frac{u_{x,a}-u_{x,b}}{h} \tag{6.105}$$

$$\frac{\partial u_y}{\partial z} = \frac{2z-h}{2\mu}\frac{\partial p}{\partial y} - \frac{u_{y,a}-u_{y,b}}{h} \tag{6.106}$$

$$u_x = \frac{z(z-h)}{2\mu}\frac{\partial p}{\partial x} + \frac{h-z}{h}u_{x,a} + \frac{z}{h}u_{x,b} \tag{6.107}$$

$$u_y = \frac{z(z-h)}{2\mu}\frac{\partial p}{\partial y} + \frac{h-z}{h}u_{y,a} + \frac{z}{h}u_{y,b} \tag{6.108}$$

The viscous shear stresses are defined by

$$\tau_{zx} = \mu\left(\frac{\partial u_z}{\partial x} + \frac{\partial u_x}{\partial z}\right) \tag{6.109}$$

$$\tau_{zy} = \mu\left(\frac{\partial u_z}{\partial y} + \frac{\partial u_y}{\partial z}\right) \tag{6.110}$$

The order of magnitude of $\partial u_z/\partial x$ and $\partial u_z/\partial y$ are much smaller than $\partial u_x/\partial z$ and $\partial u_y/\partial z$, so the viscous shear stresses can be approximated by

$$\tau_{zx} = \mu\frac{\partial u_x}{\partial z} \tag{6.111}$$

$$\tau_{zy} = \mu\frac{\partial u_y}{\partial z} \tag{6.112}$$

From Equations 6.105 and 6.106, the viscous shear stresses acting on the solid surfaces can be expressed by

$$(\tau_{zx})_{z=0} = \left(\mu\frac{\partial u_x}{\partial z}\right)_{z=0} = -\frac{h}{2}\frac{\partial p}{\partial x} - \frac{\mu(u_{x,a}-u_{x,b})}{h} \tag{6.113}$$

$$(-\tau_{zx})_{z=h} = -\left(\mu\frac{\partial u_x}{\partial z}\right)_{z=h} = -\frac{h}{2}\frac{\partial p}{\partial x} + \frac{\mu(u_{x,a}-u_{x,b})}{h} \tag{6.114}$$

$$(\tau_{zy})_{z=0} = \left(\mu\frac{\partial u_y}{\partial z}\right)_{z=0} = -\frac{h}{2}\frac{\partial p}{\partial y} - \frac{\mu(u_{y,a}-u_{y,b})}{h} \tag{6.115}$$

$$(-\tau_{zy})_{z=h} = -\left(\mu\frac{\partial u_y}{\partial z}\right)_{z=h} = -\frac{h}{2}\frac{\partial p}{\partial y} + \frac{\mu(u_{y,a} - u_{y,b})}{h} \tag{6.116}$$

The negative signs for the viscous shear stresses, in Equations 6.113 to 6.116, indicate that the stress acts in a direction opposite to the motion.

The volumetric flow rates per unit width in the x and y directions are defined by

$$q_x = \int_0^h u_x dz \tag{6.117}$$

$$q_y = \int_0^h u_y dz \tag{6.118}$$

Substituting for the velocity components using Equations 6.107 and 6.108 in Equations 6.117 and 6.118 gives

$$q_x = -\frac{h^3}{12\mu}\frac{\partial p}{\partial x} + \frac{u_{x,a} + u_{x,b}}{2}h \tag{6.119}$$

$$q_y = -\frac{h^3}{12\mu}\frac{\partial p}{\partial y} + \frac{u_{y,a} + u_{y,b}}{2}h \tag{6.120}$$

The Reynolds equation is formed by substituting the expressions for the volumetric flow rate into the continuity equation.

Integrating the continuity equation gives

$$\int_0^h \left[\frac{\partial \rho}{\partial t} + \frac{\partial}{\partial x}(\rho u_x) + \frac{\partial}{\partial y}(\rho u_y) + \frac{\partial}{\partial z}(\rho u_z)\right] dz = 0 \tag{6.121}$$

The integral

$$\int_0^h \frac{\partial}{\partial x}[f(x,y,z)]dz = -f(x,y,h)\frac{\partial h}{\partial x} + \frac{\partial}{\partial x}\left[\int_0^h f(x,y,z)dz\right] \tag{6.122}$$

If the density is assumed to be the mean density of the fluid across the film, then the u_x term in Equation 6.121 is

$$\int_0^h \frac{\partial}{\partial x}(\rho u_x)dz = -(\rho u_x)_{z=h}\frac{\partial h}{\partial x} + \frac{\partial}{\partial x}\left(\int_0^h \rho u_x dz\right) = -\rho u_{x,b}\frac{\partial h}{\partial x} + \frac{\partial}{\partial x}\left(\int_0^h \rho u_x dz\right) \tag{6.123}$$

Similarly, for the u_y term in Equation 6.121,

$$\int_0^h \frac{\partial}{\partial y}(\rho u_y)dz = -\rho u_{y,b}\frac{\partial h}{\partial y} + \frac{\partial}{\partial y}\left(\int_0^h \rho u_y dz\right) \tag{6.124}$$

The u_z term can be integrated directly giving

$$\int_0^h \frac{\partial}{\partial z}(\rho u_z)dz = \rho(u_{z,b} - u_{z,a}) \tag{6.125}$$

The integral form of the continuity equation, Equation 6.121, on substitution of Equations 6.123-6.125, can be stated as

$$h\frac{\partial \rho}{\partial t} - \rho u_{x,b}\frac{\partial h}{\partial x} + \frac{\partial}{\partial x}\left(\rho \int_0^h u_x dz\right) - \rho u_{y,b}\frac{\partial h}{\partial y} + \frac{\partial}{\partial y}\left(\rho \int_0^h u_y dz\right) + \rho(u_{z,b} - u_{z,a}) = 0 \tag{6.126}$$

The integrals in Equation 6.126 represent the volumetric flow rates per unit width. Substitution of the values for these integrals from Equations 6.119 and 6.120 gives the general Reynolds equation.

$$\frac{\partial}{\partial x}\left(-\frac{\rho h^3}{12\mu}\frac{\partial p}{\partial x}\right) + \frac{\partial}{\partial y}\left(-\frac{\rho h^3}{12\mu}\frac{\partial p}{\partial y}\right) + \frac{\partial}{\partial x}\left[\frac{\rho h(u_{x,a}+u_{x,b})}{2}\right] + \frac{\partial}{\partial y}\left[\frac{\rho h(u_{y,a}+u_{y,b})}{2}\right] + \rho(u_{z,b}-u_{z,a}) - \rho u_{x,b}\frac{\partial h}{\partial x} - \rho u_{y,b}\frac{\partial h}{\partial y} + h\frac{\partial p}{\partial t} = 0 \tag{6.127}$$

The first two terms of Equation 6.127 are the Poiseuille terms and describe the net flow rates due to pressure gradients within the lubricated area. The third and fourth terms are the Couette terms and describe the net entrained flow rates due to surface velocities. The fifth to the seventh terms are due to a squeezing motion. The eighth term describes the net flow rate due to local expansion as a result of density changes with time. Equation 6.127 is repeated below ,with the identification of the various terms emphasized.

$$\underbrace{\frac{\partial}{\partial x}\left(-\frac{\rho h^3}{12\mu}\frac{\partial p}{\partial x}\right) + \frac{\partial}{\partial y}\left(-\frac{\rho h^3}{12\mu}\frac{\partial p}{\partial y}\right)}_{\text{Poiseuille}} + \underbrace{\frac{\partial}{\partial x}\left[\frac{\rho h(u_{x,a}+u_{x,b})}{2}\right] + \frac{\partial}{\partial y}\left[\frac{\rho h(u_{y,a}+u_{y,b})}{2}\right]}_{\text{Couette}} + \underbrace{\rho(u_{z,b}-u_{z,a}) - \rho u_{x,b}\frac{\partial h}{\partial x} - \rho u_{y,b}\frac{\partial h}{\partial y}}_{\text{Squeeze}} + \underbrace{h\frac{\partial p}{\partial t}}_{\substack{\text{Net flow due to} \\ \text{local expansion}}} = 0$$

For tangential only motion, where

$$u_{z,b} = u_{x,b}\frac{\partial h}{\partial x} + u_{y,b}\frac{\partial h}{\partial y} \tag{6.128}$$

and $u_{z,a} = 0$, Equation 6.127 reduces to

$$\frac{\partial}{\partial x}\left(\frac{\rho h^3}{\mu}\frac{\partial p}{\partial x}\right)+\frac{\partial}{\partial y}\left(\frac{\rho h^3}{\mu}\frac{\partial p}{\partial y}\right)=12\overline{u}_x\frac{\partial(\rho h)}{\partial x}+12\overline{u}_y\frac{\partial(\rho h)}{\partial y} \tag{6.129}$$

where

$$\overline{u}_x=\frac{u_{x,a}+u_{x,b}}{2}=\text{constant} \tag{6.130}$$

$$\overline{u}_y=\frac{u_{y,a}+u_{y,b}}{2}=\text{constant} \tag{6.131}$$

For hydrodynamic lubrication, the fluid properties do not vary significantly through the bearing and can be considered constant. In addition for hydrodynamic lubrication, the motion is pure sliding and $\overline{u}_y=0$.

The Reynolds equation can therefore be simplified to

$$\frac{\partial}{\partial x}\left(h^3\frac{\partial p}{\partial x}\right)+\frac{\partial}{\partial y}\left(h^3\frac{\partial p}{\partial y}\right)=12\overline{u}_x\mu_o\frac{\partial h}{\partial x} \tag{6.132}$$

In some lubrication applications, side leakage can be neglected, and Equation 6.129 can be restated as

$$\frac{\partial}{\partial x}\left(\frac{\rho h^3}{\mu}\frac{\partial p}{\partial x}\right)=12\overline{u}_x\frac{\partial(\rho h)}{\partial x} \tag{6.133}$$

Equation 6.133 can be integrated giving

$$\frac{1}{\mu}\frac{dp}{dx}=\frac{12\overline{u}_x}{h^2}+\frac{A}{\rho h^3} \tag{6.134}$$

With boundary conditions $dp/dx = 0$ when $x = x_m$, $\rho = \rho_m$, $h = h_m$ gives $A=-12\overline{u}_x\rho_m h_m$. The subscript m refers to the condition for which $dp/dx = 0$ such as the point of maximum pressure. Substituting for A in Equation 6.134 gives

$$\frac{dp}{dx}=12\overline{u}_x\mu\frac{\rho h-\rho_m h_m}{\rho h^3} \tag{6.135}$$

If the density can be considered constant, then Equation 6.135 becomes

$$\frac{dp}{dx}=12\overline{u}_x\mu\frac{h-h_m}{h^3} \tag{6.136}$$

For the case of a gas-lubricated bearing, the density, using the ideal gas law, is given by

$$\rho=\frac{p}{RT} \tag{6.137}$$

From Equation 6.129, and taking the viscosity as constant,

$$\frac{\partial}{\partial x}\left(\rho h^3\frac{\partial p}{\partial x}\right)+\frac{\partial}{\partial y}\left(\rho h^3\frac{\partial p}{\partial y}\right)=12\overline{u}_x\mu_o\frac{\partial(\rho h)}{\partial x} \tag{6.138}$$

Expressing Equation 6.129 in cylindrical coordinates

$$\frac{\partial}{\partial r}\left(\frac{r\rho h^3}{\mu}\frac{\partial p}{\partial r}\right)+\frac{1}{r}\frac{\partial}{\partial \phi}\left(\frac{\rho h^3}{\mu}\frac{\partial p}{\partial \phi}\right)=12\left[\overline{u}_r\frac{\partial(\rho r h)}{\partial r}+\overline{u}_\phi\frac{\partial(\rho h)}{\partial \phi}\right] \tag{6.139}$$

where

$$\overline{u}_r=\frac{u_{r,a}+u_{r,b}}{2} \tag{6.140}$$

$$\overline{u}_\phi=\frac{u_{\phi,a}+u_{\phi,b}}{2} \tag{6.141}$$

If the viscosity and density can be assumed to be constant, then Equation 6.139 becomes

$$\frac{\partial}{\partial r}\left(rh^3\frac{\partial p}{\partial r}\right)+\frac{1}{r}\frac{\partial}{\partial \phi}\left(h^3\frac{\partial p}{\partial \phi}\right)=12\mu_o\left[\overline{u}_r\frac{\partial(rh)}{\partial r}+\overline{u}_\phi\frac{\partial h}{\partial \phi}\right] \tag{6.142}$$

Equation 6.142 applies to a thrust bearing where the fluid film is in the z direction and the bearing dimensions are in the r, ϕ directions.

For turbulent flow, the Reynolds equation is

$$\frac{\partial}{\partial x}\left(\frac{h^3}{\mu k_x}\frac{\partial \overline{p}}{\partial x}\right)+\frac{\partial}{\partial y}\left(\frac{h^3}{\mu k_y}\frac{\partial \overline{p}}{\partial y}\right)=\frac{\overline{u}_x}{2}\frac{\partial h}{\partial x} \tag{6.143}$$

where (from Constantinescu, 1962)

$$k_x=12+0.026\left(\frac{\rho\Omega r h}{\mu}\right)^{0.102} \tag{6.144}$$

$$k_y=12+0.0198\left(\frac{\rho\Omega r h}{\mu}\right)^{0.091} \tag{6.145}$$

For an infinitely wide journal bearing, the pressure in the axial direction can be assumed to be constant. This approach is valid for a length to diameter ratio of $L/D > 2$. The integrated form of the Reynolds Equation, Equation 6.136, on substitution for $\overline{u}_x=(u_a+u_b)/2=\Omega a/2$, as $u_b=0$ for a stationary bearing surface, gives

$$\frac{dp}{dx}=\frac{6\mu_o a\Omega(h-h_m)}{h^3} \tag{6.146}$$

$$dx=ad\phi \tag{6.147}$$

$$\frac{dp}{d\phi}=\frac{6\mu_o a^2\Omega(h-h_m)}{h^3} \tag{6.148}$$

$$\cos\alpha=\frac{1}{b}[h+a+e\cos(\pi-\phi)] \tag{6.149}$$

$$h = b\cos\alpha - a + e\cos\phi \tag{6.150}$$

Hence, using trigonometric relationships,

$$h = b\left[1-\left(\frac{e}{b}\right)^2\sin^2\phi\right]^{0.5} - a + e\cos\phi \tag{6.151}$$

Expanding the series

$$\left[1-\left(\frac{e}{b}\right)^2\sin^2\phi\right]^{0.5} = 1-\frac{1}{2}\left(\frac{e}{b}\right)^2\sin^2\phi - \frac{1}{8}\left(\frac{e}{b}\right)^4\sin^4\phi - \ldots \tag{6.152}$$

Hence

$$h = b\left[1-\frac{1}{2}\left(\frac{e}{b}\right)^2\sin^2\phi - \frac{1}{8}\left(\frac{e}{b}\right)^4\sin^4\phi - \ldots\right] - a + e\cos\phi \tag{6.153}$$

$$\mathrm{b} - \mathrm{a} = \mathrm{c} \tag{6.154}$$

$$h = c + e\left[\cos\phi - \frac{1}{2}\left(\frac{e}{b}\right)\sin^2\phi - \frac{1}{8}\left(\frac{e}{b}\right)^3\sin^4\phi - \ldots\right] \tag{6.155}$$

The ratio e/b is typically of the order of 1×10^{-3}. As a result, terms in Equation 6.155 with this ratio can readily be neglected, giving

$$h = c + e\cos\phi = c\left(1 + \frac{e}{c}\cos\phi\right) = c(1 + \varepsilon\cos\phi) \tag{6.156}$$

where ε is the eccentricity ratio defined by

$$\varepsilon = \frac{e}{c} \tag{6.157}$$

Substitution of Equation 6.156 in Equation 6.148 gives

$$\frac{dp}{d\phi} = 6\,\mu\Omega\left(\frac{a}{c}\right)^2\left[\frac{1}{(1+\varepsilon\cos\phi)^2} - \frac{h_m}{c(1+\varepsilon\cos\phi)^3}\right] \tag{6.158}$$

Integration of Equation 6.158 gives the following expression for the pressure distribution.

$$p = 6\mu\Omega\left(\frac{a}{c}\right)^2\int\left[\frac{1}{(1+\varepsilon\cos\phi)^2} - \frac{h_m}{c(1+\varepsilon\cos\phi)^3}\right]d\phi + A \tag{6.159}$$

where A is a constant of integration.

For a journal bearing,

$$x = a\phi \tag{6.160}$$

and

$$\overline{u} = \frac{u_{x,a}}{2} = \frac{a\Omega}{2} \tag{6.161}$$

From Equation 6.132,

$$\frac{\partial}{\partial\phi}\left(h^3\frac{\partial p}{\partial\phi}\right) + a^2\frac{\partial}{\partial y}\left(h^3\frac{\partial p}{\partial y}\right) = 6\mu_o\Omega a^2\frac{\partial h}{\partial\phi} \tag{6.162}$$

Substituting for the film thickness gives

$$\frac{\partial}{\partial\phi}\left(h^3\frac{\partial p}{\partial\phi}\right) + a^2h^3\frac{\partial^2 p}{\partial y^2} = -6\mu_o\Omega a^2 e\sin\phi \tag{6.163}$$

The Reynolds equation, for example, Equation 6.163 or 6.129, can be solved by approximate mathematical methods or numerically. Once the pressure distribution has been established, the journal performance can be determined in terms of the bearing load capacity, frictional losses, lubricant flow requirements, and the lubricant temperature rise. Use can be made of a series of design charts that relate numerical solutions to key characteristic parameters. The solutions and accompanying charts presented here were originally produced by Raimondi and Boyd (1958a, b, c) who used an iterative technique to solve the Reynolds equations. These charts give the film thickness, coefficient of friction, lubricant flow, lubricant side flow ratio, minimum film thickness location, maximum pressure ratio, maximum pressure ratio position, and film termination angle versus the Sommerfield number (see Figures 6.24 to 6.31).

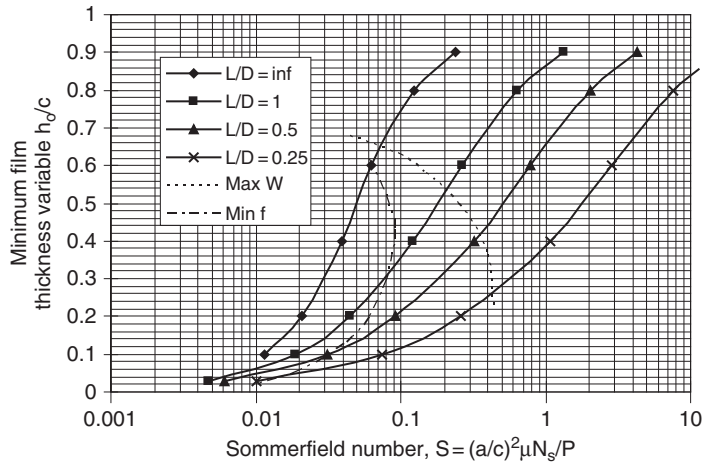

FIGURE 6.24 Chart for the minimum film thickness variable, (h_o/c) versus the Sommerfield number (data from Raimondi and Boyd, 1958c).

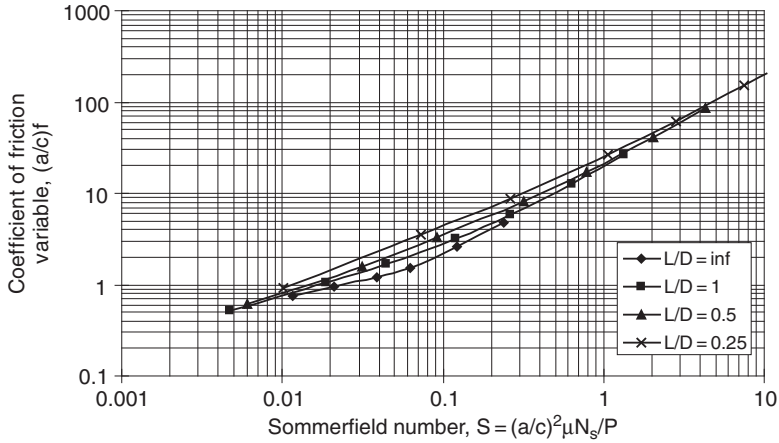

FIGURE 6.25 Chart for determining the coefficient of friction variable, $(a/c)f$ (data from Raimondi and Boyd, 1958c).

The Sommerfield number, which is also known as the bearing characteristic number, is defined in Equation 6.164. It is used as it encapsulates all the parameters usually defined by the designer, such as the journal radius, clearance, viscosity, rotational speed, and load. Great care needs to be taken with units in the design of journal bearings. Many design charts have been produced using English units (psi, reyn, Btu, etc.). As long as a consistent set of units is maintained, use of the charts will yield sensible results. In particular, note the use of revolutions per second in the definition of speed in the Sommerfield number given in Equation 6.164.

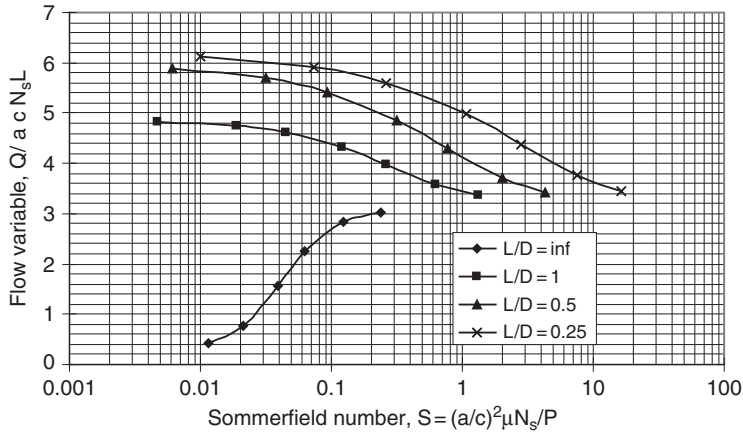

FIGURE 6.26 Chart for determining the flow variable, $Q/(acN_sL)$ (data from Raimondi and Boyd, 1958c).

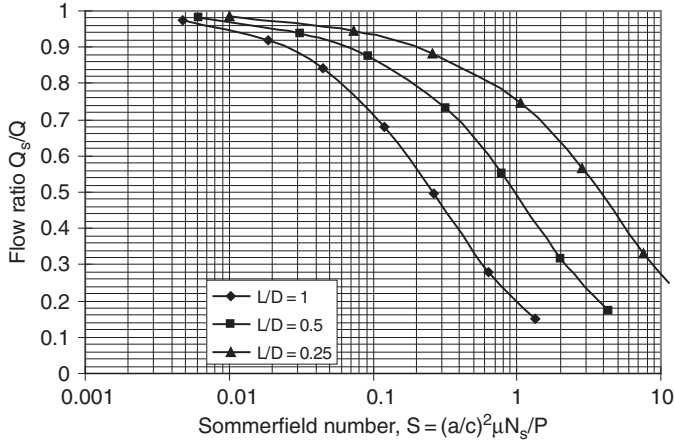

FIGURE 6.27 Chart for determining the ratio of side flow, Q_s, to total flow, Q (data from Raimondi and Boyd, 1958c).

$$S = \left(\frac{a}{c}\right)^2 \frac{\mu N_s}{P} \tag{6.164}$$

where: S is the bearing characteristic number

a is the journal radius, (m)
c is the radial clearance (m)
μ is the absolute viscosity (Pa s)
N_s is the journal speed (revolutions per second, rps)

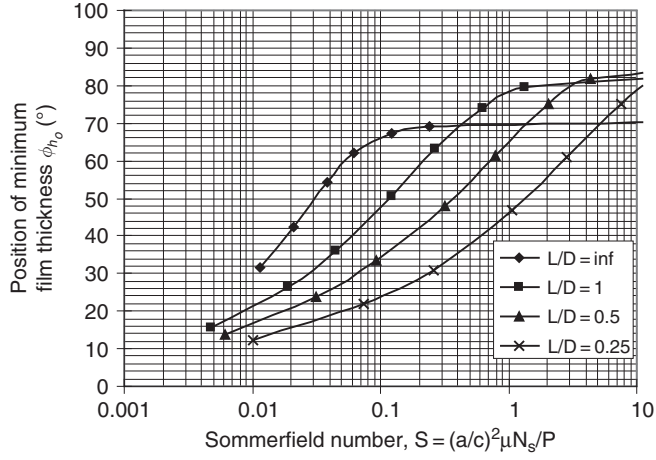

FIGURE 6.28 Chart for determining the position of the minimum film thickness ϕ_{ho} (data from Raimondi and Boyd, 1958c).

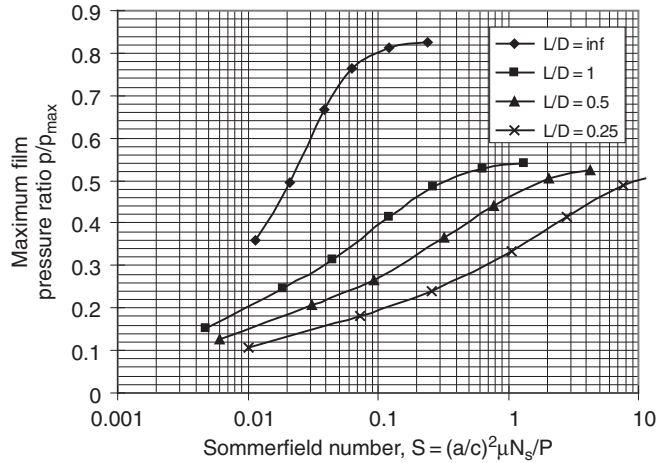

FIGURE 6.29 Chart for determining the maximum film pressure ratio, p/p_{max} (data from Raimondi and Boyd, 1958c).

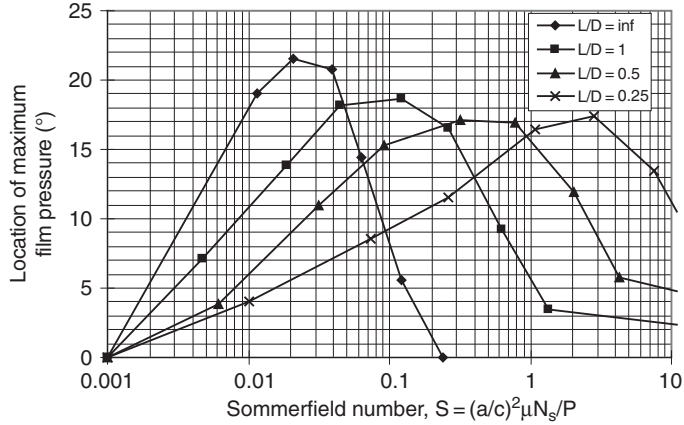

FIGURE 6.30 Chart for determining the position of maximum pressure, $\phi_{p_{max}}$ (data from Raimondi and Boyd, 1958c).

$P = W/LD$ is the load per unit of projected bearing area (N/m^2)
W is the load on the bearing (N),
D is the journal diameter (m),
L is the journal bearing length (m).

Consider the journal shown in Figure 6.32. As the journal rotates, it will pump lubricant in a clockwise direction. The lubricant is pumped into a wedge-shaped space, and the journal is forced over to the opposite side. The angular position where the lubricant film is at its minimum thickness h_o is called the attitude angle, ϕ_{h_o}.

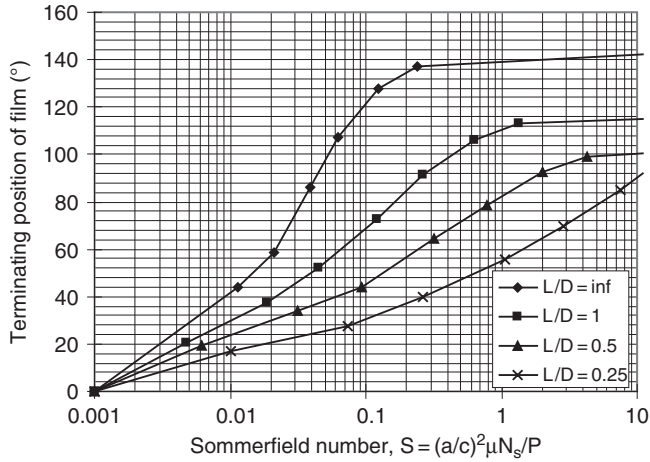

FIGURE 6.31 Chart for determining the film termination angle, ϕ_{p_o} (data from Raimondi and Boyd, 1958c).

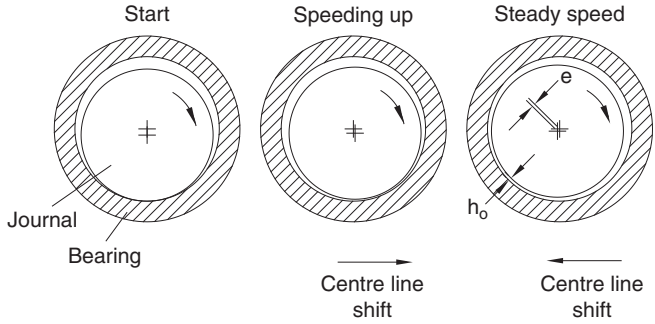

FIGURE 6.32 Full film hydrodynamic bearing motion from start-up.

The center of the journal is displaced from the center of the bearing by a distance e called the eccentricity. The ratio of the eccentricity e to the radial clearance c is called the eccentricity ratio ($\varepsilon = e/c$), Equation 6.157. The relationship between the film thickness, clearance, eccentricity, and eccentricity ratio are defined in Equations 6.165 and 6.166.

$$h_o = c - e \tag{6.165}$$

$$\frac{h_o}{c} = 1 - \varepsilon \tag{6.166}$$

One assumption made in the Raimondi and Boyd analysis is that the viscosity of the lubricant is constant as it passes through the bearing. However, work is done on the lubricant in the bearing, and the temperature of the lubricant

leaving the bearing zone will be higher than the entrance value. Figure 6.18 shows the variation of viscosity with temperature for some of the SAE and ISO defined lubricants, and it can be seen that the value of the viscosity for a particular lubricant is highly dependent on the temperature. Some of the lubricant entrained into the bearing film emerges as side flow that carries away some of the heat. The remainder flows through the load-bearing zone and carries away the remainder of the heat generated. The temperature used for determining the viscosity can be taken as the average of the inlet and exit lubricant temperatures as given by Equation 6.167.

$$T_{av} = T_1 + \frac{T_2 - T_1}{2} = T_1 + \frac{\Delta T}{2} \tag{6.167}$$

where T_1 is the temperature of the lubricant supply and T_2 is the temperature of the lubricant leaving the bearing. Generally, petroleum lubrication oils should be limited to a maximum temperature of approximately 70 ^{o}C in order to prevent excessive oxidation.

One of the parameters that needs to be determined is the bearing lubricant exit temperature T_2. This is a trial-and-error or iterative process. A value of the temperature rise, ΔT, is guessed, the viscosity for a standard oil, corresponding to this value, determined, and the analysis performed. If the temperature rise calculated by the analysis does not correspond closely to the guessed value, the process should be repeated using an updated value for the temperature rise until the two match. If the temperature rise is unacceptable, it may be necessary to try a different lubricant or to modify the bearing configuration.

Given the length, the journal radius, the radial clearance, the lubricant type, and its supply temperature, the steps for determining the various bearing operating parameters are listed below.

1. Determine the speed of the journal and the load to be supported.
2. If L and D are not already determined, set the proportions of the bearing so that the load capacity, $P = W/LD$, is somewhere between 0.34 MN/m^2 for light machinery and 13.4 MN/m^2 for heavy machinery.
3. Determine a value for the radial clearance of the bearing using the data presented in Figure 6.22.
4. If not already specified, select a lubricant. Lubricant oil selection is a function of speed or compatibility with other lubricant requirements. Generally, as the design speed rises, oils with a lower viscosity should be selected.
5. Estimate a value for the temperature rise ΔT across the bearing. The value taken for the initial estimate is relatively unimportant. As a guide, a value of $\Delta T = 10\,^{o}$C is generally a good starting guess. This value can be increased for high-speed bearings and for low-bearing clearances.
6. Determine the average lubricant temperature $T_{av} = T_1 + \Delta T/2$ and find the corresponding value for the viscosity for the chosen lubricant.

7. Calculate the Sommerfield number, $S = (a/c)^2 \mu N_s / P$ and the length to diameter ratio (L/D).
8. Use the charts (Figures 6.25, 6.26, and 6.27) to determine values for the coefficient of friction variable, the total lubricant flow variable, and the ratio of the side flow to the total lubricant flow with the values for the Sommerfield number and the L/D ratio.
9. Calculate the temperature rise of the lubricant through the bearing using

$$\Delta T = \frac{8.30 \times 10^{-6} P}{1 - \frac{1}{2}(Q_s/Q)} \times \frac{(a/c) f}{Q/acN_s L} \tag{6.168}$$

10. If this calculated value does not match the estimated value for ΔT to within, say, 1 °C, repeat the procedure from step 6 using the updated value of the temperature rise to determine the average lubricant temperature.
11. Check that the values for the Sommerfield number and the length to diameter ratio give a design that is in the optimal operating region for minimal friction and maximum load capability on the chart for the minimum film thickness variable (between the dashed lines in Figure 6.24). If the operating Sommerfield number and L/D ratio combination do not fall within this zone, then it is likely that the bearing design can be improved by altering the values for c, L, D, the lubricant type, and the operating temperature as appropriate.
12. If the value for the temperature rise across the bearing has converged, values for the total lubricant flow rate, Q, the side flow rate Q_s and the coefficient of friction f can be calculated. The journal bearing must be supplied with the value of the total lubricant calculated in order for it to perform as predicted by the charts.
13. The charts given in Figures 6.24 to 6.31 can be used to determine values for the maximum film thickness, the maximum film pressure ratio, the location of the maximum film pressure, and its terminating angular location as required.
14. The torque required to overcome friction in the bearing can be calculated by

$$T_q = fWa \tag{6.169}$$

15. The power lost in the bearing is given by

$$\text{Power} = \Omega \times T_q = 2\pi N_s \times T_q \tag{6.170}$$

where Ω is the angular velocity (rad/s).

16. Specify the surface roughness for the journal and bearing surfaces. A ground journal with an arithmetic average surface roughness of 0.4 to 0.8 μm is recommended for bearings of good quality. For high-precision equipment both surfaces can be lapped or polished to give a surface

roughness of 0.2 to 0.4 μm. The specified roughness should be less than the minimum film thickness.

17. Design the recirculation and sealing system for the bearing lubricant.

For values of the length to diameter (L/D) ratio other than those shown in the charts given in Figures 6.24–6.31, values for the various parameters can be found by interpolation using Equation 6.171 (see Raimondi and Boyd, 1958b).

$$y = \frac{1}{(L/D)^3}\left[\begin{array}{l} -\frac{1}{8}\left(1-\frac{L}{D}\right)\left(1-2\frac{L}{D}\right)\left(1-4\frac{L}{D}\right)y_\infty \\ +\frac{1}{3}\left(1-2\frac{L}{D}\right)\left(1-4\frac{L}{D}\right)y_1-\frac{1}{4}\left(1-\frac{L}{D}\right)\left(1-4\frac{L}{D}\right)y_{1/2} \\ +\frac{1}{24}\left(1-\frac{L}{D}\right)\left(1-2\frac{L}{D}\right)y_{1/4} \end{array}\right] \tag{6.171}$$

Here y is the desired variable and y_∞, y_1, $y_{1/2,}$ and $y_{1/4}$ are the variables at $L/D = \infty$, 1, ½, and ¼, respectively.

Example 6.10.

A full journal bearing has a nominal diameter of 30.0 mm and a bearing length of 30.0 mm (see Figure 6.33). The bearing supports a load of 900 N, and the journal design speed is 10000 rpm. The radial clearance has been specified as 0.04 mm. An ISO VG22 oil, with a density of 900 kg/m^3, has been chosen, and the lubricant supply temperature is 60 °C.

Find the temperature rise of the lubricant, the lubricant flow rate, the minimum film thickness, the torque required to overcome friction, and the heat generated in the bearing.

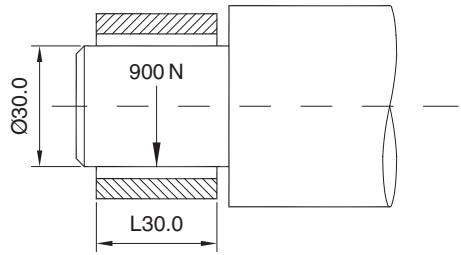

FIGURE 6.33 Bearing design example.

Solution

The primary data are $D = 30.0$ mm, $L = 30$ mm, $W = 900$ N, $N = 10000$ rpm, $c = 0.04$ mm, ISO VG 22, $T_1 = 60\ ^{o}$C.

Guess a value for the lubricant temperature rise ΔT across the bearing to be, say, $\Delta T = 15\ ^{o}$C.

$$T_{av} = T_1 + \frac{\Delta T}{2} = 60 + \frac{15}{2} = 67.5\ ^{o}\text{C}$$

From Figure 6.18 for ISO VG22 at 67.5 ^{o}C, $\mu = 0.0068$ Pa s.

The mean radius is given by

$$r_m = \frac{a+b}{2} = 15.02 \text{ mm}$$

$$b - a = 0.04 \text{ mm}$$

$$\nu = \mu/\rho = 0.0068/900 = 7.556 \times 10^{-6}\text{m}^2/\text{s}$$

So the Taylor number using this approximate value for the kinematic viscosity is given by

$$Ta_m = \frac{\Omega r_m^{0.5}(b-a)^{1.5}}{\nu} = 4.296$$

As this is much less than the critical Taylor number, 41.19, laminar flow can be assumed.

$$N_s = 10000/60 = 166.7\text{rps}, L/D = 30/30 = 1$$

$$P = \frac{W}{LD} = \frac{900}{0.03 \times 0.03} = 1 \times 10^6\ \text{N/m}^2$$

$$S = \left(\frac{a}{c}\right)^2 \frac{\mu N_s}{P} = \left(\frac{15 \times 10^{-3}}{0.04 \times 10^{-3}}\right)^2 \frac{0.0068 \times 166.7}{1 \times 10^6} = 0.1594$$

From Figure 6.25 with $S = 0.1594$ and $L/D = 1$, $(a/c)f = 4.0$
From Figure 6.26 with $S = 0.1594$ and $L/D = 1$, $Q/(acN_sL) = 4.2$
From Figure 6.27 with $S = 0.1594$ and $L/D = 1$, $Q_s/Q = 0.62$

The value of the temperature rise of the lubricant can now be calculated using Equation 6.168:

$$\Delta T = \frac{8.3 \times 10^{-6} P}{1 - 0.5\frac{Q_s}{Q}} \times \frac{\frac{r}{c} f}{\frac{Q}{rcN_S L}} = \frac{8.3 \times 10^{-6} \times 1 \times 10^6}{1 - (0.5 \times 0.62)} \times \frac{4.0}{4.2} \approx 11.5\ ^{o}\text{C}$$

As the value calculated for the lubricant temperature rise is significantly different from the estimated value, it is necessary to repeat the above calculation but using the new improved estimate for determining the average lubricant temperature.

Using $\Delta T = 11.5\ ^{o}\text{C}$ to calculate T_{av} gives:

$$T_{av} = 60 + \frac{11.5}{2} = 65.7\ ^{o}\text{C}$$

Repeating the procedure using the new value for T_{av} gives:

$\mu = 0.007$ Pa s

$S = 0.1641$

From Figure 6.25 with $S = 0.1641$ and $L/D = 1$, $(a/c)f = 4.0$
From Figure 6.26 with $S = 0.1641$ and $L/D = 1$, $Q/(acN_sL) = 4.2$
From Figure 6.27 with $S = 0.1641$ and $L/D = 1$, $Q_s/Q = 0.61$

$$\Delta T = \frac{8.3 \times 10^{-6} \times 2.4 \times 10^{6}}{1-(0.5 \times 0.61)} \times \frac{4.0}{4.2} \approx 11.4\ ^{o}\text{C},$$

$$T_{av} = 60 + \frac{11.4}{2} = 65.7\ ^{o}\text{C}$$

This value for T_{av} is the same as the previous calculated value, suggesting that the solution has converged. For $T_{av} = 65.7\ ^{o}\text{C}$, $\mu = 0.007$ Pa s, and $S = 0.1641$.

The other parameters can now be found.

$$Q = acN_sL \times 4.2 = 15 \times 0.04 \times 166.7 \times 30 \times 4.2 = 12600\ \text{mm}^3/\text{s}$$

From Figure 6.24 $h_o/c = 0.48$. $h_o = 0.0192$ mm.

An indication of the Reynolds number can be obtained from

$$Re_x = \frac{\rho_o u_{x,o} h_o^2}{\mu_o l_o} = \frac{900 \times (1047 \times 0.01502) \times (0.0192 \times 10^{-3})^2}{0.007 \times 0.01502} = 0.04963$$

$$f = 4.0 \times (c/r) = 4.0 \times (0.04/15) = 0.01067$$

The torque is given by $T_q = fWa = 0.01067 \times 900 \times 0.015 = 0.144$ N m.

The power dissipated in the bearing is given by Power $= 2\pi \times T_q \times N_s = 150.8$ W.

Example 6.11.

A full journal bearing is required for a 30-mm-diameter shaft, rotating at 2750 rpm supporting a load of 2000 N (see Figure 6.34). From previous experience, the lubrication system available is capable of delivering the lubricant to the bearing at 50 °C. Select an appropriate radial clearance, length, and lubricant for the bearing and determine the temperature rise of the lubricant, the total lubricant flow rate required, and the power absorbed in the bearing. Check that your chosen design operates within the optimum zone indicated by the dotted lines on the minimum film thickness ratio chart (Figure 6.24).

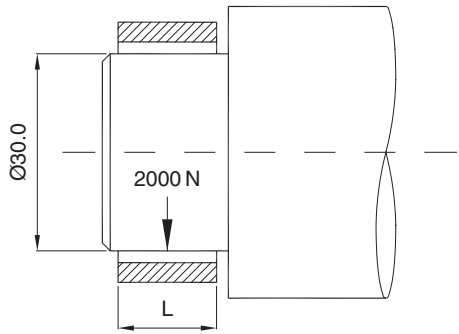

FIGURE 6.34 Bearing design example.

Solution

The primary design information is: $D = 30.0$ mm, $W = 2000$ N, $N = 2750$ rpm, $T_1 = 50\ ^{o}$C.

From Figure 6.22 for a speed of 2750 rpm and a nominal journal diameter of 30 mm, a suitable value for the diametral clearance is 0.05 mm. The radial clearance is therefore 0.025 mm. The next step is to set the length of the bearing. Typical values for L/D ratios are between 0.5 and 1.5. Here a value for the ratio is arbitrarily set as $L/D = 0.5$ to give a compact bearing, that is, L =15 mm. If this value is found to be unsuitable, it can be adjusted.

Given the speed of the bearing, 2750 rpm, as an initial proposal an SAE 10 lubricant is selected.

The procedure for determining the average lubricant temperature is the same as that for the previous example. As a first estimate, the temperature rise of the lubricant is taken as 10 ^{o}C, and the results of the iterative procedure are given in Table 6.3.

The mean radius is given by

$$r_m = \frac{a+b}{2} = \frac{15 + 15.025}{2} = 15.01 \text{ mm}$$

$$b - a = 0.025 \text{ mm}$$

An estimate for the kinematic viscosity can be found, taking the average temperature of the oil as 55 ^{o}C and assuming a density of 900 kg/m^3. At 55 ^{o}C, the viscosity for SAE 10 is approximately 0.016 Pa.s

$$\nu = \mu/\rho = 0.016/900 = 1.78 \times 10^{-5} \text{m}^2/\text{s}$$

So the Taylor number using this approximate value for the kinematic viscosity is given by

$$Ta_m = \frac{\Omega r_m^{0.5}(b-a)^{1.5}}{\nu} = 0.2481$$

As this is much less than the critical Taylor number, 41.19, laminar flow can be assumed.

$$P = \frac{W}{LD} = \frac{2000}{0.015 \times 0.03} = 4.444 \times 10^6 \text{ N/m}^2$$

$$S = \left(\frac{a}{c}\right)^2 \frac{\mu N_s}{P} = \left(\frac{15 \times 10^{-3}}{0.025 \times 10^{-3}}\right)^2 \frac{\mu 45.83}{4.444 \times 10^6} = 3.713\,\mu.$$

$$T_{av} = T_1 + \frac{\Delta T}{2} = 50 + \frac{10}{2} = 55\ ^\circ\text{C}$$

Values for ΔT, T_{av}, μ, S, $(a/c)f$, Q/acN_sL, Q_s/Q from successive iterations using steps 6–10 of the calculation procedure are given in Table 6.3.

The total lubricant flow rate required is given by $Q = acN_sL \times 5.62 = 15 \times 0.025 \times 45.83 \times 15 \times 5.62 = 1449\,\text{mm}^3/\text{s}$.

With $S = 0.04084$ and $L/D = 0.5$, the design selected is within the optimum operating zone for minimum friction and optimum load capacity indicated in Figure 6.24.

The friction factor, $f = 1.95 \times (c/a) = 1.95 \times 0.025/15 = 0.00325$.

$T_q = fWa = 0.00325 \times 2000 \times 0.015 = 0.0975$ N m
$Power = 2\pi N_s \times T_q = 28.08$ W

TABLE 6.3 Tabular data for Example 6.11

Temperature rise, ΔT (°C)	10	29.11	24.40	23.81
Average lubricant temperature T_{av} (°C)	55	64.6	62.2	61.9
Average lubricant viscosity μ (Pa s)	0.016	0.012	0.011	0.011
Sommerfield number, S	0.0594	0.04455	0.04084	0.04084
Coefficient of friction variable $(a/c)f$	2.4	2.0	1.95	1.95
Flow variable Q/acN_sL	5.58	5.6	5.62	5.62
Side flow to total flow ratio Q_s/Q	0.91	0.92	0.925	0.925

6.6. ROTATING CYLINDERS AND SPHERES WITH CROSS-FLOW

A cylinder that is rotating about its axis and moving through a fluid in a direction perpendicular to its axis will experience a force perpendicular to both the direction of motion and the axis as illustrated in Figures 6.35 and 6.36. The production of lift forces by a rotating cylinder placed in a fluid stream

is known as the Magnus effect, after Heinrich Magnus who investigated inaccuracies when firing cannonballs (Magnus, 1852).

An explanation of the Magnus effect can be developed by considering the schematic diagrams in Figures 6.35, 6.36, and 6.37. At the surface of the cylinder, fluid will rotate at the tangential velocity component of the cylinder's outer radius due to the no slip condition, and the action of viscosity will transmit that rotation to adjacent layers of fluid. This boosts the velocity of the fluid stream in the direction of rotation and opposes it in the reverse direction;

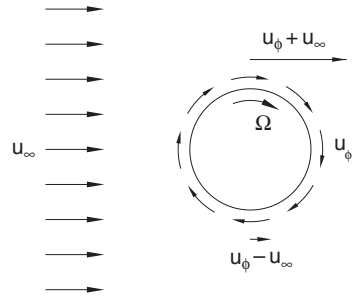

FIGURE 6.35 A rotating cylinder in a fluid stream cross-flow.

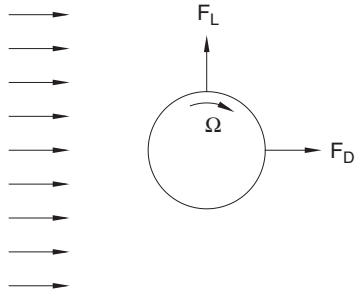

FIGURE 6.36 Lift and drag forces on a rotating cylinder in a fluid stream.

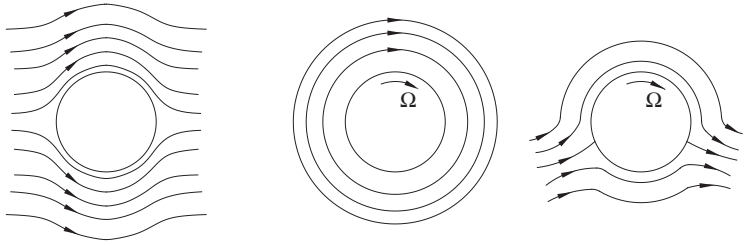

FIGURE 6.37 Flow patterns for (a) a circular cylinder placed in a parallel flow, (b) pure circulatory flow, and (c) combined viscous and circulatory flow.

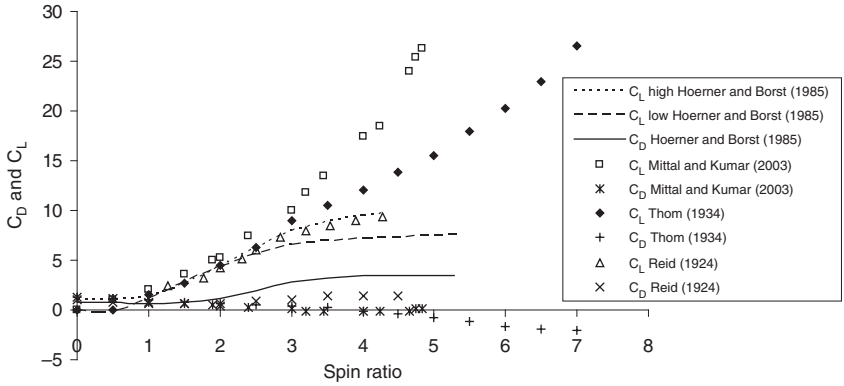

FIGURE 6.38 Lift and drag coefficients, C_L and C_D, for rotating cylinder in a cross-flow as a function of spin ratio, $\Omega r/u\infty$ (data from Hoerner and Borst, 1985; Mittal and Kumar, 2003; Thom, 1934; Reid, 1924.

see Figure 6.35. For a nonrotating cylinder in fluid stream, the flow field will be as illustrated in Figure 6.37a. Pure circulatory flow, resulting from rotation, will give a flow pattern of concentric circles as indicated in Figure 6.37b. Superimposing these two flow fields and plotting the streamlines by vector addition gives the flow field shown in Figure 6.37c. If the flow has been deflected to the right, then an acceleration has occurred, and therefore an associated force has caused this. The reaction to the force will therefore cause a force on the cylinder as shown in Figure 6.36 at right-angles to the fluid stream.

Lift and drag coefficients for a spinning cylinder in a cross-flow are presented in Figure 6.38 as a function of the spin ratio, the ratio of the surface speed to the free-stream flow speed, using data from Reid (1924), Thom (1934), Hoerner and Borst (1985), and Mittal and Kumar (2003). The definitions used for the lift and drag coefficients for the data presented are given in Equations 6.172 and 6.173. From potential flow theory, the lift per unit length of a rotor is 2π times the product of the tangential velocity component of the rotor and the free-stream flow speed. Discs or fences can be added to a cylinder to reduce tip vortices, in a manner that is comparable to the use of fences and the end of wing tips on aircraft. The data from Thom (1934) presented in Figure 6.38 is for a rotating cylinder with multiple disc fences along the length of the cylinder placed at intervals of 0.75 times the rotor diameter.

$$C_L = \frac{Lift}{0.5\rho U^2 DL} \tag{6.172}$$

$$C_D = \frac{Drag}{0.5\rho U^2 DL} \tag{6.173}$$

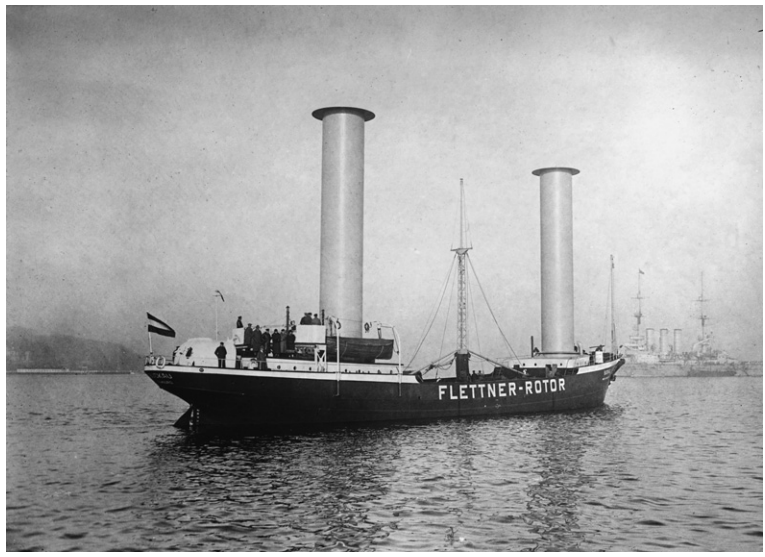

FIGURE 6.39 The Buckau with two 18-m-high and 2.7-m-diameter rotors.

Anton Flettner in the 1920s proposed the use of rotating cylinders, instead of sails, to propel ships, with motors driving large cylinders mounted on the ship's deck and the wind providing the parallel flow necessary to induce a propulsive force as a result of the interaction between the wind and the rotating cylinders. Anton Flettner built two ships based on this principle. In 1926, the three-masted schooner rig on the 52-m *Buckau* was replaced by two rotors, shown in Figure 6.39, and the ship was subsequently renamed the *Baden-Baden*. Each rotor was 18 m high and 2.7 m in diameter. The ship's performance exceeded all expectations, being faster than before and able to sail much closer to the wind.

The *Baden-Baden* successfully crossed the Atlantic in 1926 (see Seufert and Seufert, 1983). As a result of this success, the Transportation Department of the German Navy ordered the construction of another rotor ship, the *Barbara*, shown in Figure 6.40. The *Barbara* was 92 m long and was fitted with three rotors, each 17 m high, 4 m in diameter, and driven at 150 rpm by a 27-kW electric motor. The *Barbara* carried 3000 tons of cargo and a few passengers and operated between Hamburg and Italy for six years, further proving the technical viability of the concept. Of course, if there is no wind, then there is no cross-flow and a ship becomes becalmed with such a system.

Example 6.12.

Determine the force applied to each rotor by the wind for the *Barbara* rotor ship. Take the diameter of the rotors to be 4 m, length 17 m, and a rotor speed of 150 rpm. Assume that the speed of the wind relative to the rotor is 7 m/s.

FIGURE 6.40 The Barbara with three, 17-m-high, 4-m-diameter rotors.

Solution

The angular velocity of each rotor is

$$\Omega = 150 \times \frac{2\pi}{60} = 15.71 \text{ rad/s}$$

The spin ratio is

$$\frac{\Omega r}{u_{z=\infty}} = \frac{15.71 \times (4/2)}{7} = 4.488$$

From Figure 6.38, $C_L = 8.7$ and $C_D = 3.45$.
Assuming a density of 1.2047 kg/m^3, the lift and drag forces are

$$\text{Lift} = \frac{1}{2}\rho U^2 D L C_L = 0.5 \times 1.2047 \times 7^2 \times 4 \times 17 \times 8.7 = 17460 \text{ N}$$

$$\text{Drag} = \frac{1}{2}\rho U^2 D L C_D = 0.5 \times 1.2047 \times 7^2 \times 4 \times 17 \times 3.45 = 6924 \text{ N}$$

The resultant force applied to each rotor is therefore

$$\sqrt{17460^2 + 7025^2} = 18780 \text{ N}$$

This acts at an angle of

$$tan^{-1}\left(\frac{6924}{17460}\right) = 21.63^\circ \text{ to the left of the relative wind direction.}$$

Salter, Sortino, and Latham (2008) have proposed the use of rotor ships to propel a fleet of 1500 ships for the purpose of spraying a fine mist of seawater spray worldwide to alter the Earth's albedo and as a result affect the energy balance due to insolation and radiation to space. The concept is to offset the effects of the presumed 3.7 W/m^2 heating rise apportioned to worldwide industrial activity. A concept design for a spray vessel is shown in Figure 6.41. For the vessel shown, the wind would be blowing from the right-hand side of the image, the rotor angular velocity would be clockwise as viewed from above, and the resulting rotor thrust would be to the left.

A rotating sphere moving through a stream of fluid also experiences a force perpendicular to both the axis of rotation and the motion. The flow structure is considerably more complex than that of the equivalent two-dimensional cross-sectional rotating cylinder. Experimental data for the case of a smooth spinning sphere in a uniform flow is given in Figure 6.42 as a function of the spin ratio. The Reynolds number is of secondary importance. At low values of the spin ratio, the lift is negative. Above a spin ratio of approximately 0.5, the lift becomes positive and increases, with the spin ratio leveling off to an approximately constant value of lift coefficient equal to about 0.35 for spin ratios above about 1.5.

Spin has little effect on the drag coefficient, which ranges from about 0.5 to 0.65 for spin ratios up to about 5. For large values of the spin ratio the flow behavior can be understood using concepts similar to those described for the rotating cylinder case. Any quantitative data, however, needs to be derived from experiment. At low values of the spin ratio, the force reverses in direction. This effect is probably due to transition occurring in the boundary layer on the side where the relative velocity between the sphere and the fluid is higher. As transition delays separation, this will produce a flow of the form shown in Figure 6.43, with the flow deflected to the side where separation has occurred earliest. The deflection of the wake in this way produces a resultant force that is opposite to that of the conventional Magnus effect.

The phenomenon of variable lift and drag with spin rate is familiar in sports. In tennis and ping-pong, the spin rate is used to control the trajectory and bounce of a shot. A golf ball can be driven off a tee with a speed of the order of 90 m/s with a backspin of 9000 rpm. The spin results in an increase in the lift coefficient that substantially increases the range of the shot. In baseball the pitcher uses spin to throw a curve ball. Considerable interest in the science associated with sports has resulted in a substantial quantity of data becoming available. The general aerodynamics of sports balls is reviewed by Mehta (1985). Specific studies, for example, on cricket balls are reported by Mehta and Wood (1980) and Mehta et al. (1983); baseballs by Briggs (1959) and Watts and Sawyer (1975); and golf balls by Beerman and Harvey (1976), Smits (1994), and Beasley and Camp (2002).

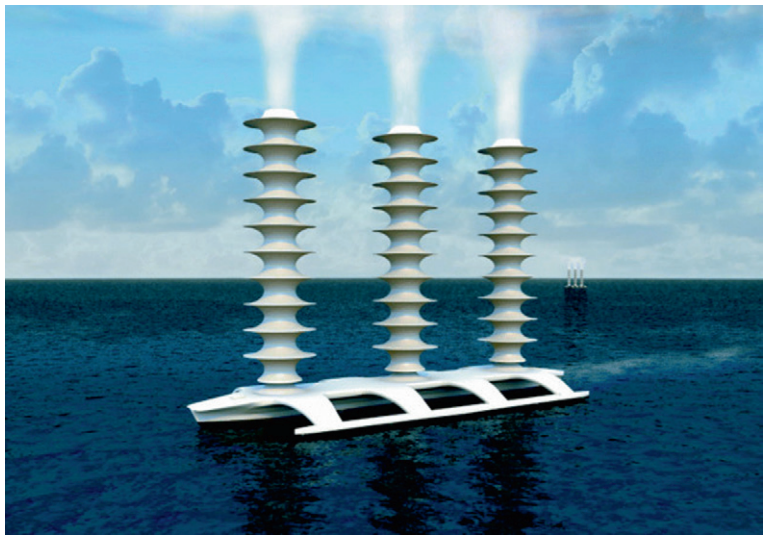

FIGURE 6.41 Concept design for a Flettner rotor spray vessel to alter the Earth's albedo. After J MacNeill (2006).

Example 6.13.

Determine the radius of curvature at maximum elevation in the vertical plane for a smooth tennis ball that is hit at 24 m/s with a topspin of 7800 rpm. Determine the comparable radius of curvature if the ball is hit with no spin. The radius of the tennis ball is 32.8 mm, and its mass is 57 g. A smooth tennis ball has been assumed for simplicity.

Solution

The Reynolds number based on the forward speed and ball diameter is given by

$$Re_D = \frac{\rho u D}{\mu} = \frac{1.2047 \times 24 \times 0.0656}{1.819 \times 10^{-5}} = 1.043 \times 10^5$$

The spin ratio is

$$\frac{\Omega r}{u_{z=\infty}} = \frac{7800 \times (2\pi/60) \times 0.0328}{24} = 1.116$$

From Figure 6.42, $C_L \approx 0.3$
The lift force is given by

$$F_L = 0.5\rho U^2 A C_L = 0.5\rho U^2 \pi r^2 C_L = 0.5 \times 1.205 \times 24^2 \pi \times 0.0328^2 \times 0.3 \approx 0.35 \text{ N}$$

As the ball is hit with topspin, this force will act downward, causing the ball to drop faster than it would otherwise.

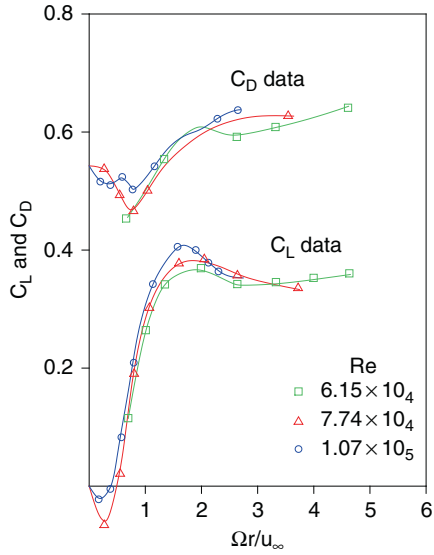

FIGURE 6.42 Lift and drag coefficients for a smooth spinning sphere in a uniform flow (data from Maccoll, 1928).

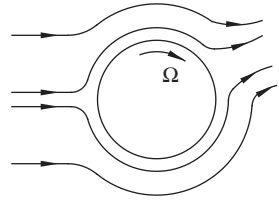

FIGURE 6.43 Flow pattern for a smooth spinning sphere in a uniform flow at low values of spin ratio.

From Newton's second law,

$$\sum F = -F_L - mg = ma_z = -m\frac{u^2}{R}$$

Hence the radius of curvature is given by

$$R = \frac{u^2}{(F_L/m) + g} = \frac{24^2}{(0.35/0.057) + 9.81} = 36.1 \text{ m}$$

In the absence of spin,

$$\sum F = -mg = ma_z = -m\frac{u^2}{R}$$

Hence the radius of curvature is given by

$$R = \frac{u^2}{g} = \frac{24^2}{9.81} = 58.7 \text{ m}$$

Comparison of these figures shows that topspin makes the ball drop faster, creating many tactical advantages, such as allowing a player to hit harder and higher over the net or to make the ball dip at an oncoming net-rusher's feet.

6.7. CONCLUSIONS

The flow phenomenon in rotating cylinder applications depends on the orientation of the cylinder to the flow and the axis of rotation. Correlations are available to determine the drag associated with rotating shaft applications. For an annulus where the inner or outer cylinder may be rotating, consideration can be given to the stability of the flow in order to identify whether vortices are likely to form. Under certain conditions of inner cylinder rotation or combined inner and outer cylinder rotation, toroidal vortices can form in an annulus known as Taylor vortices, with alternate vortices rotating in opposite directions.

Rotation of a cylinder or sphere in a cross-flow causes a deflection of the fluid stream and as a result a force due to reaction on the cylinder or sphere concerned. This phenomenon can be exploited to provide a propulsive mechanism for ships and boats using winds to provide the cross-flow; in sports, the variability in lift and drag with spin rate is exploited to control the trajectory and bounce of a shot and in some cases to provide ball or projectile flight paths that are more difficult to predict.

REFERENCES

Andereck, C.D., and Hayot, F. (eds.). *Ordered and turbulent patterns in Taylor Couette flow.* Plenum, 1992.

Beasley, D., and Camp, T. Effects of dimple design on the aerodynamic performance of a golf ball. In E. Thain (ed.), *Science and Golf* IV, pp. 328–340. Routledge, 2002.

Beerman, P.W., and Harvey, J.K. Golf ball aerodynamics. *Aeronaut. Quarterly*, 27 (1976), pp. 112–122.

Bilgen, E., and Boulos, R. Functional dependence of torque coefficient of coaxial cylinders on gap width and Reynolds numbers. *Trans. ASME, Journal of Fluids Engineering* (1973), pp. 122–126.

Briggs, L.J. Effect of spin and speed on the lateral deflection of a baseball and the Magnus effect for smooth spheres. *American Journal of Physics*, 27 (1959), pp. 589–596.

Chandrasekhar, S. Hydrodynamic stability of viscid flow between coaxial cylinders. *Proceedings of the National Academy of Sciences*, 46 (1960b), pp. 141–143.

Chandrasekhar, S. The hydrodynamic stability of inviscid flow between coaxial cylinders. *Proceedings of the National Academy of Sciences*, 46 (1960a), pp. 137–141.

Childs, P.R.N., and Noronha, M.B. The impact of machining techniques on centrifugal compressor performance. ASME Paper 97-GT-456, 1997.

Childs, P.R.N. *Mechanical design.* 2nd Edition. Elsevier, 2004.

Coles, D. Transition in circular Couette flow. *Journal of Fluid Mechanics*, 21 (1965), pp. 385–425.

Consantinescu, V.N.Analysis of bearings operating in turbulent regime. Transactions of the ASME, Journal of Basic Engineering, 84(1962), pp. 139–151.

Couette, M. Etudes sur le frottement des liquids. *Ann. Chim. Phys.* Ser. 6, 21 (1890), pp. 433–510.

Di Prima, R.C., and Swinney, H. Instabilities and transition in flow between concentric rotating cylinders. In Swinney, H. and Gollub, J.P. (eds.), *Hydrodynamic instabilities and the transition to turbulence*, pp. 139–180. Springer 1981.

Donnelly, R.J. Experiments on the stability of viscous flow between rotating cylinders. I. Torque measurements. *Proc. Royal Society*, London, Ser. A, 246 (1958), pp. 312–325.

Donnelly, R.J., and Fultz, D. Experiments on the stability of viscous flow between rotating cylinders. II. Visual observations. *Proc. Royal Society*, London, Ser. A (1960), 258, pp. 101–123.

Donnelly, R.J., and Schwarz, K.W. Experiments on the stability of viscous flow between rotating cylinders. VI. Finite amplitude experiments. *Proc. Royal Society*, London, Ser. A, 283 (1965), pp. 531–556.

Donnelly, R.J. and Simon, N.J. An empirical torque relation for supercritical flow between rotating cylinders, *Journal of Fluid Mechanics*, 7 (1960), pp. 401–418.

Fenstermacher, P.R., Swinney, H.L., and Gollub, J.P. Dynamical instabilities and the transition to chaotic Taylor vortex flow. *Journal of Fluid Mechanics*, 94 (1979), pp. 103–129.

Gollub, J.B., and Swinney, H.L. Onset of turbulence in a rotating fluid. *Physical Review Letters*, 35 (1975), pp. 927–930.

Hamrock, B.J. *Fundamentals of fluid film lubrication.* McGraw-Hill, 1994.

Harrison, W.J. The hydrodynamical theory of lubrication with special reference to air as a lubricant. *Trans. Cambridge Philos. Soc*., xxii (1912–1925), pp. 6–54, 1913.

Hendriks, F. On Taylor vortices and Ekman layers in flow-induced vibration of hard disk drives. Microsystem Technologies-Micro-and Nanosystems-Information Storage and Processing Systems, Vol. 16, 2010, pp. 93–101.

Hoerner, S.F., and Borst H.V. Fluid-dynamic lift. Information on lift and its derivatives, in air and in water. Hoerner Fluid Dynamics, 1985.

Hoffmann, C., Altmeyer, S., Pinter, A., and Lucke, M. Transitions between Taylor vortices and spirals via wavy Taylor vortices and wavy spirals. *New Journal of Physics*, 11 (2009).

International Organization for Standardization. ISO 3448 Industrial liquid lubricants—ISO viscosity classification. 1992.

Kaye, J., and Elgar, E.C. Modes of adiabatic and diabatic fluid flow in an annulus with an inner rotating cylinder. *Trans. ASME* (1958), pp. 753–765.

Lamb, H. *Hydrodynamics*. 6th Edition, Cambridge University Press, 1932.

Lewis, J.W. Experimental study of the motion of a viscous liquid contained between two coaxial cylinders. *Proc. Royal Society,* London, Series A, 117 (1927), pp. 388–407.

Maccoll, J.W.. Aerodynamics of a spinning sphere. *Journal of the Royal Aeronautical Society*, 32 (1928), pp. 777–798.

MacNeill, J. www.johnmacneill.com Last accessed 17th July 2010.

Magnus, G. *Abhandlung der Akademie der Wissenschaftern*. Berlin, 1852.

Mallock, A. Determination of the viscosity of water. *Proc. Royal Society*, London, Ser. A, 45 (1888), pp. 126–132.

Mallock, A. Experiments on fluid viscosity. *Philos. Trans. Royal Society*, London, Ser. A, 187 (1896), p. 41–56.

Mehta, R.D. The aerodynamics of sports balls. *Annual Review of Fluid Mechanics*, 17 (1985), pp. 151–189.

Mehta, R.D., Bentley, K., Proudlove, M., and Varty, P. Factors affecting cricket ball swing. *Nature*, 303 (1983), pp. 787–788.

Mehta, R.D., and Wood, D.H. Aerodynamics of the cricket ball. *New Scientist*, 87 (1980), pp. 442–447.

Mittal, S., and Kumar, B. Flow past a rotating cylinder. *Journal of Fluid Mechanics*, 476 (2003), pp. 303–334.

Moalem, D., and Cohen, S. Hydrodynamics and heat/mass transfer near rotating surfaces. *Advances in Heat Transfer*, 21, pp. 141–183. Academic Press, 1991.

Neale, M.J. (ed.). *The tribology handbook*. Butterworth Heinemann, 1995.

Nissan, A.H., Nardacci, J.L., and Ho, L.Y. The onset of different modes of instability for flow between rotating cylinders. *American Institute of Chemical Engineers Journal*, 9 (1963), pp. 620–624.

Raimondi, A.A., and Boyd, J. A solution for the finite journal bearing and its application to analysis and design: I. *ASLE Transactions*, 1 (1958a), pp. 159–174.

Raimondi, A.A., and Boyd, J. A solution for the finite journal bearing and its application to analysis and design: II. *ASLE Transactions*, 1 (1958b), pp. 175–193.

Raimondi, A.A., and Boyd, J. A solution for the finite journal bearing and its application to analysis and design: III. *ASLE Transactions*, 1 (1958c), pp. 194–209.

Rayleigh, Lord. On the dynamics of revolving fluids. *Proc. Royal Society*, London, Ser. A, 93 (1916), pp. 148–154.

Reid, E.G. Tests of rotating cylinders. NACA Technical Note, NACA-TN-209, 1924.

Reynolds, O. On the theory of lubrication and its application to Mr Beauchamp Tower's experiments including an experimental determination of the viscosity of olive oil. *Philos. Trans. Royal Society*, 177 (1886), pp. 157–234.

Roberts, P.H. Appendix in experiments on the stability of viscous flow between rotating cylinders, VI. Finite amplitude experiments. *Proc. Royal Society*, London, Series A, 238 (1965), pp. 531–556.

Salter, S., Sortino, G., and Latham, J. Sea-going hardware for the cloud albedo method of reversing global warming. *Philos. Trans. Royal Society* A, 366 (2008), pp. 3989–4006.

Schultz-Grunow, F. Stabilitat einer rotierended flussigkeit. *Zeitschrift für angewandte Mathematik Mechanik* (1963), pp. 411–415.

Schwarz, K.W., Springnett, B.E., and Donnelly, R.J. Modes of instability in spiral flow between rotating cylinders. *Journal of Fluid Mechanics*, 20 (1964), pp. 281–289.

Seufert, W., and Seufert, S. Critics in a spin over Flettner's ship. *New Scientist* (1983), pp. 656–659.

Smits, A.J. A new aerodynamic model of a golf ball in flight. In A.J. Cochran and M.R. Farrally, (eds.), *Science and Golf* II, pp. 340–347. E&FN Spon, 1994.

Snyder, H.A. Change in wave form and mean flow associated with wave length variations in rotating Couette flow. *Journal of Fluid Mechanics*, Part L, 35 (1969), pp. 337–352.

Snyder, H.A. Waveforms in rotating Couette flow. *International Journal of Heat and Non-linear Mechanics*, 5 (1970), pp. 659–685.

Sparrow, E.M., Munro, W.D., and Johnson, V.K. Instability of the flow between rotating cylinders: the wide gap problem. *Journal of Fluid Mechanics*, 20 (1964), pp. 35–46.

Steinheuer, J. Three dimensional boundary layers on rotating bodies and in corners. AGARD No. 97 (1965), pp. 567–611.

Taylor, G.I. Stability of a viscous liquid contained between two rotating cylinders. *Proc. Royal Society*, London, Ser. A, 223 (1923), pp. 239–343.

Theodorsen, T., and Regier, A. Experiments on drag of revolving discs, cylinders and streamline rods at high speeds. NACA Report 793, 1944.

Thom, A. Effects of discs on the air forces on a rotating cylinder. Aeronautical Research Committee Reports and Memoranda 1623, 1934.

Walowit, J., Tsao, S., and Di-Prima, R.C. Stability of flow between arbitrarily spaced concentric cylindrical surfaces including the effect of a radial temperature gradient. *Trans. Journal of Applied Mechanics*, 31 (1964), pp. 585–593.

Watts, R.G., and Sawyer, E. Aerodynamics of a knuckleball. *American Journal of Physics*, 43 (1975), pp. 960–963.

Welsh, R.J. *Plain bearing design handbook*. Butterworth, 1983.